AIMS Environmental Science

AIMS Environmental Science, 13(1): 179–216.
DOI: 10.3934/environsci.2026008
Received: 04 October 2025
Revised: 28 January 2026
Accepted: 13 February 2026
Published: 6 March 2026

https://www.aimspress.com/journal/environmental

Research article

Flood susceptibility evaluation of arid coastal basins along the Northwest Coast of Egypt

Rasha Hosny[1], Mohamed M.S Mabrouk[2] and Mohamed A.H Eizeldin[3,4,*]

[1] Water Engineering Department, Faculty of Engineering, Heliopolis University for Sustainable Development; rasha.hosny@hu.edu.eg
[2] Head of Hydrology and Hydraulics Department, Saden Company, Egypt; moh.m.shaaban1995@gmail.com
[3] Assistant Prof., Civil Engineering Dept., Faculty of Engineering of Mataria, Helwan University
[4] Civil Engineering Dept., Faculty of Engineering, The British University in Egypt, Cairo Governorate 11837, Egypt; mohamed.eizeldin@bue.edu.eg

* **Correspondence:** Email: mohamed.eizeldin@bue.edu.eg; Tel: +201021186000.

Abstract: Flash floods are among the most critical natural hazards in arid regions, where limited infiltration capacity and intense episodic rainfall generate rapid runoff and severe flooding. Egypt's Northwest Coast, particularly the Sallum–Alexandria corridor, faces growing flood risks under changing climatic conditions, posing challenges to sustainable water and land management. In this study, we present an integrated assessment of flood hazard severity and geomorphological susceptibility across seven major arid coastal basins (>500 km²) using an integrated framework of Geographic Information Systems (GIS), remote sensing (RS), and hydrological and hydraulic modeling. Basin morphometry was derived from SRTM-based DEMs and analyzed through WMS 11.0 to extract 45 parameters describing geometry, drainage, relief, and texture. Rainfall trend analysis (1979–2020) demonstrated a significant increase in precipitation intensity over the last decade, with HYFRAN-PLUS employed to estimate 100-year return periods. Hydrological simulations revealed Basin 2 (Wadi El-Harika) produced the highest peak discharge (800 m³/s), while Basins 6 and 7 generated minimal runoffs. Conversely, hydraulic modeling indicated that Basins 5, 6, and 7 experienced the greatest inundation depths (up to 30 m), highlighting a disconnect between runoff volume and flood severity due to local topographic and drainage conditions. The results emphasized the need for basin-specific analysis and demonstrated that flood hazard severity could not be inferred from runoff magnitude alone. The proposed integrated framework provided a robust physical basis for

flood hazard and geomorphological susceptibility assessment in arid coastal basins and offers a foundation for future flood risk or vulnerability analyses through the incorporation of exposure and adaptive capacity indicators.

Keywords: climate change; flash floods; hydrological and hydraulic modeling; flood hazard assessment; geomorphological susceptibility; arid and semi-arid basins; northwest coast of Egypt

1. Introduction

Flash floods are rapid, localized floods characterized by the sudden and unexpected rise of water levels, typically within a few hours, often generated by intense rainfall or dam failures [1]. They are a significant hazard worldwide, causing widespread damage and loss of life [2]. The increasing frequency and severity of flash floods are closely linked to climate change, which intensifies extreme weather events and disrupts regional hydrological patterns [3].

Flash floods are a recurrent phenomenon in arid regions like Egypt, often triggered by short-lived but intense storms. These high-intensity rain events have emerged as one of the most destructive and widespread natural hazards in Egypt over the past decade [4]. Due to ongoing water scarcity challenges, the Egypt's National Water Research Plan for 2017–2037 prioritizes optimizing the use of all water sources, including stormwater and flood runoff to address the growing imbalance between water supply and demand [5]. Flood events can significantly disrupt human activities and impose heavy economic burdens, particularly in terms of mitigation and response costs [6]. Several variables that influence the severity of flash floods were determined, including the nature of the storm system, which were most commonly convective and frontal types [6]. Other contributing factors include the intensity and duration of rainfall, water loss through infiltration and evaporation, and the physical structure and hierarchy of the drainage basins. The quick response to a heavy rainfall event depends mainly on the basin's geomorphometric features [7]. According to studies, the risk of floods has grown due to extreme precipitation events, unplanned changes in land cover, and excessive melting of glaciers and snow [8,9]. Flash-flood problems in Egypt have largely increased due to factors such as the continuous changing in land use/land cover, urbanization activities, expansion in flash-flood prone areas, low-quality constructions, the increasing of the urbanization density, and the effects of global climate change [4,6]. The most influential contributors to flooding are natural factors such as hydrological and meteorological features, geological structures, soil types, geomorphology, and vegetation [10]. The growing population and socioeconomic development in the hazard zone have increased the vulnerability of flood-prone areas [11–13]. One of the essential elements of vulnerability to stressors, such as man-made or natural hazards, is susceptibility, which is a guess as to "where" the dangerous occurrence is most likely to occur [11]. Additionally, flash flood susceptibility is essentially the geospatial probability of an intense rainfall event in an area supported by geomorphometric and hydrological variables [14]. Researchers have analyzed drainage basin characteristics in arid regions globally through geomorphological techniques, largely grounded in the foundational work of Horton and Strahler [15,16]. Morphometric analysis offers valuable insights into predicting hydrological behaviors within a basin. As noted by Strahler, quantitative methods provide a systematic and objective approach for numerically describing the morphometric features of basin features that are strongly linked to surface runoff patterns [17]. This quantitative framework forms a solid basis for modeling

rainfall-runoff interactions by establishing a theoretical relationship between the basin's physical structure and its hydrological performance.

Basin morphology can be accomplished by regular procedures depending on field visits, monitoring, topographic and geologic maps, or with GIS techniques [18–20]. In the past few decades, the merging of Remote Sensing (RS) and Geographic Information System (GIS) methodologies, in conjunction with morphometric evaluation of flood susceptibility, has resulted in significant advancements that provide an accurate, valuable, and cost-effective tool for susceptibility zone planning and management [21–30]. Studies have demonstrated the effectiveness of remote sensing, GIS, and hydrological–hydraulic modeling in analyzing flash flood dynamics and hazard severity. For instance, multi-temporal satellite imagery and spatial analysis were employed to investigate flash flood events in a rapidly urbanizing environment, highlighting the combined influence of intense rainfall and surface characteristics [31]. Similarly, integrated GIS, WMS, HEC-HMS, and HEC-RAS models have been used to assess flash flood behavior and inundation patterns, illustrating the value of multi-model frameworks for identifying flood-prone areas [32]. Furthermore, climate-driven analyses based on CMIP6 projections indicate increasing variability and intensity of hydro-climatic extremes under future climate scenarios [33], emphasizing the need for rainfall trend and extreme-event analysis in flood hazard assessments. Despite these advances, arid coastal basins remain relatively underexplored, particularly with respect to the role of basin morphometry and drainage characteristics in controlling flood hazard generation.

Flash floods present a serious threat to Egypt's North Coast, often resulting in infrastructure destruction, fatalities, and substantial economic losses. The region's climatic and geographical features heighten its susceptibility to these sudden and intense flood events [34]. A major challenge in managing these hazards lies in the limited availability of detailed hydrological and meteorological data, which underscores the need for advanced technologies such as remote sensing and hydrological modeling [35]. Most of these studies suggest mitigation measures and design protective measures for such regions. The value of integrating GIS with remote sensing in the evaluation flash flood susceptibility and supporting the development of targeted risk-reduction strategies have been emphasized by researchers [36]. A case study was presented on protecting highways from flood hazards and investigating a hydrological modeling technique to assess flood risk and design culverts as a protective measure for highway infrastructure [37]. Moreover, soil conservation measures were investigated in another study to reduce surface runoff and sediment transport during heavy rainfall events in the Ras Sudr Region as a part of a mitigation measure technique to minimize the risk and severity of flash floods in vulnerable basins [38]. In addition, an integrated model using GIS, hydrological, and groundwater models was presented to design dams for flood protection, water storage, and groundwater recharge in Wadi Watier, Egypt, significantly enhancing water resources [39].

This research advances the understanding of flash flood processes along Egypt's North Coast, particularly the under-studied Sallum–Alexandria corridor, through the integration of geospatial techniques and hydrological–hydraulic modeling. Unlike other researchers who primarily focused on isolated hazard mapping, we adopt an integrated, basin-comparative perspective that emphasizes flood hazard severity and geomorphological susceptibility at the basin scale. The study distinguishes itself in three key aspects: First, by targeting a strategic yet neglected coastal zone characterized by unique climatic and geomorphological sensitivities; second, by adopting a practical approach that supports basin-specific flood mitigation and management strategies; and third, by developing a condensed methodology designed to address the constraints of limited hydrological and meteorological data.

Accordingly, our objective of this study is to assess and compare flood hazard severity and physical susceptibility across arid coastal basins along Egypt's Northwest Coast by combining remote sensing data, GIS-based morphometric analysis, hydrological simulations, and hydraulic floodplain modeling. The proposed framework provides a robust physical basis for flood hazard assessment in arid coastal environments.

2. Materials and methods

2.1. Study area

The study area is on the Northwest Coast and covers an area of about 26.3 Km^2. It is between Salloum and Alexandria between latitudes (25^O E) and (30^O E), as shown in Figure 1. The soil is composed of sandy, loamy, and clayey soils with different permeability levels, which increases the risk of flooding. The study area elevation ranges between 263 m to 1 m above the sea level, creating a gentle slope toward the coastal plain.

It is characterized by its arid to semi-arid climate, influenced by desert and coastal conditions. Precipitation is seasonal and falls from October through March during the winter, with high evaporation rates and limited surface water availability. According to the collected rainfall database, the total annual precipitation ranged from 2 to 300 mm, from 1979 to 2020 [40,41]. According to the Köppen–Geiger climate classification, this region falls within the BWh (hot desert) climate zone, characterized by scarce and highly variable rainfall [42]. These climatic conditions strongly influence runoff generation and flood processes, making the aridity of the basins a critical factor in assessing flood hazard and geomorphological susceptibility. The temperature ranges between 10–18 in the winter and 30 to 35 in the summer. The Northwest Coast region includes residential, commercial, and reclamation areas, as well as tourist villages, roads, railways, and other infrastructure. The coastal road, which runs almost parallel to the beach, is one of the basin areas. Furthermore, longitudinal roads and railways running from south to north cross the lower reaches of most drainage basins.

Figure 1. Map of Egypt and the study area.

2.2. Methodology

The core methodology of this study, illustrated in Figure 2, integrated Remote Sensing and GIS with hydrological and hydraulic modeling tools (Basin Modeling Systems (WMS), Hydrological Engineering Center- Hydrologic Modeling System (HEC-HMS), and Hydrological Engineering Center- River Analysis System (HEC-RAS)) to assess flood hazard severity and geomorphological susceptibility across the Sallum–Alexandria coastal zone. This framework combined hazard intensity metrics (rainfall, runoff, and floodplain inundation depth) with basin physical characteristics (morphometric parameters and drainage network characteristics) to identify areas prone to severe flooding. Morphometric parameters were extracted using WMS and ArcGIS based on Digital Elevation Models (DEMs), rainfall records, satellite imagery, and evaporation data to quantify susceptibility and identify critical basin features influencing flood behavior. For the hydrological component, rainfall trend analysis was conducted to identify the most critical decade of precipitation, followed by frequency analysis using Hydrological Frequency Analysis (HYFRAN-PLUS) to estimate rainfall for the maximum rainfall decade and the 100-year return period. These inputs were applied in HEC-HMS to simulate runoff hydrographs, representing basin-scale flood generation potential. Subsequently, HEC-RAS hydraulic modeling was performed to simulate floodplain inundation, producing depth and extent maps that highlight areas of highest hazard and geomorphological susceptibility. By integrating morphometric, hydrological, and hydraulic outcomes, this methodology provides a basin-specific assessment of flood hazard and physical susceptibility, offering a robust framework for comparative analysis of arid coastal basins and supporting evidence-based flood management and planning strategies along Egypt's Northwest Coast.

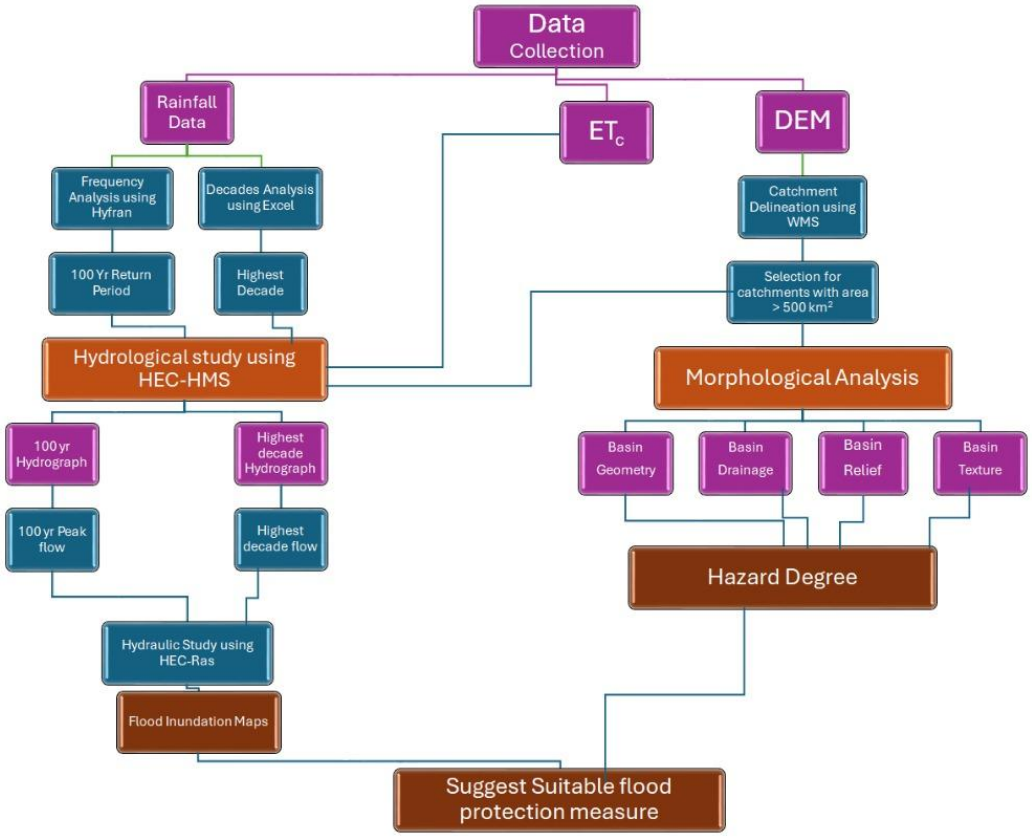

Figure 2. Methodology flowchart.

2.3. Data collection and processing

2.3.1. Digital elevation model:

The Shuttle Radar Topography Mission (SRTM) Digital Elevation Model (DEM) was downloaded from USGS website with 30 m resolution. It was georeferenced to WGS 1984- Universal Transvers Mercator (UTM) zone 36 to delineate the west north coast basins that were required for morphological and hydrological analysis. The maximum elevation was 263 m, and the minimum elevation was 0.5 m above the mean sea level.

2.3.2. Land use/land cover:

The Environmental Systems Research Institute (ESRI) land use/land cover map was used [43]. Land use/land cover is important for runoff calculation, as it is used in soil conservation services and the curve number (SCS-CN) approach. The land use of the North coast includes bare land, range land, and buildings. Most of the land is bar land while range land covers less than 25% of the study area.

2.3.3. Soil data

Another requirement for the Soil Conservation Service - Curve Number (SCS-CN) approach was the soil classification of the study area into hydrological soil groups, from A to D, using a soil classification map downloaded from Food and Agriculture Organization (FAO) website [44]. The map was clipped for the study area, and the hydrological soil groups were extracted using ArcGIS 10.3.

2.3.4. Rainfall data

A total of 67 rain gages were downloaded for the period from 1979 to 2014 [40]. The time series for some identified rainfall gages that appeared in the selected basins were completed to year 2020 [41]. Figure 3 represents the locations of the selected stations.

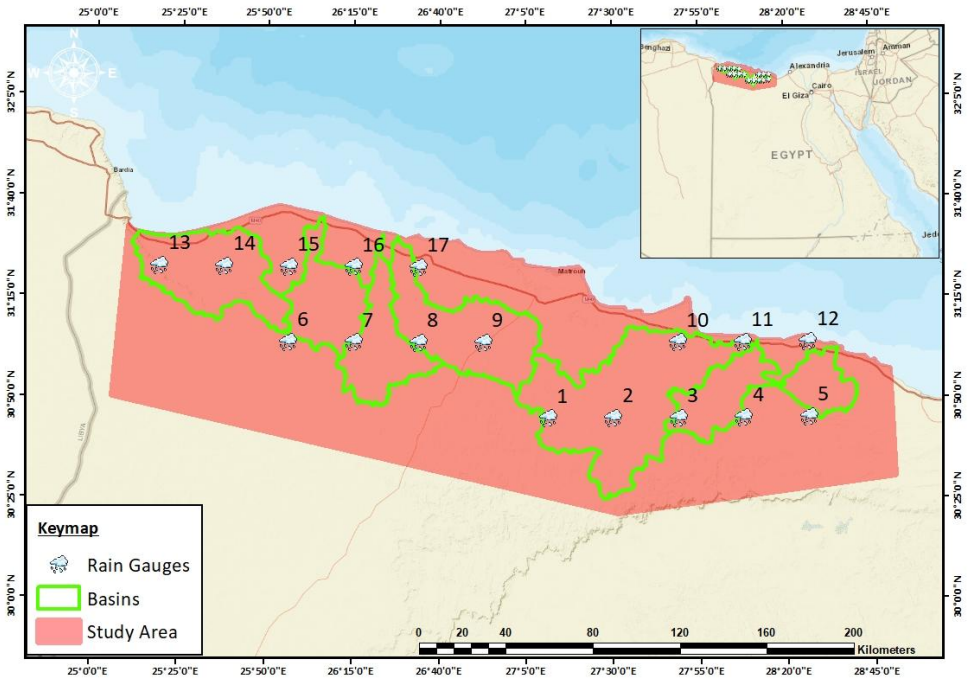

Figure 3. Locations of the selected stations.

Figure 4 shows an example of the downloaded data and represents the average daily rainfall from 2014 to 2020, showing a highly variable and irregular rainfall pattern typical of arid to semi-arid regions. It also shows that rainfall occurrences are primarily concentrated in the winter months, with significant peaks surpassing 10 mm, with late 2018 to early 2019 being the most severe, indicating the possibility of flash flood conditions. While certain years, such as 2017, recorded relatively low rainfall, a marked increase in the frequency and intensity of rainfall is evident post-2017, suggesting a potential alteration in regional precipitation trends. This pattern reinforces concerns regarding climate change's impact on more extreme and clustered rainfall events, highlighting the urgent need for updated flood risk evaluations and adaptive water management strategies in susceptible regions.

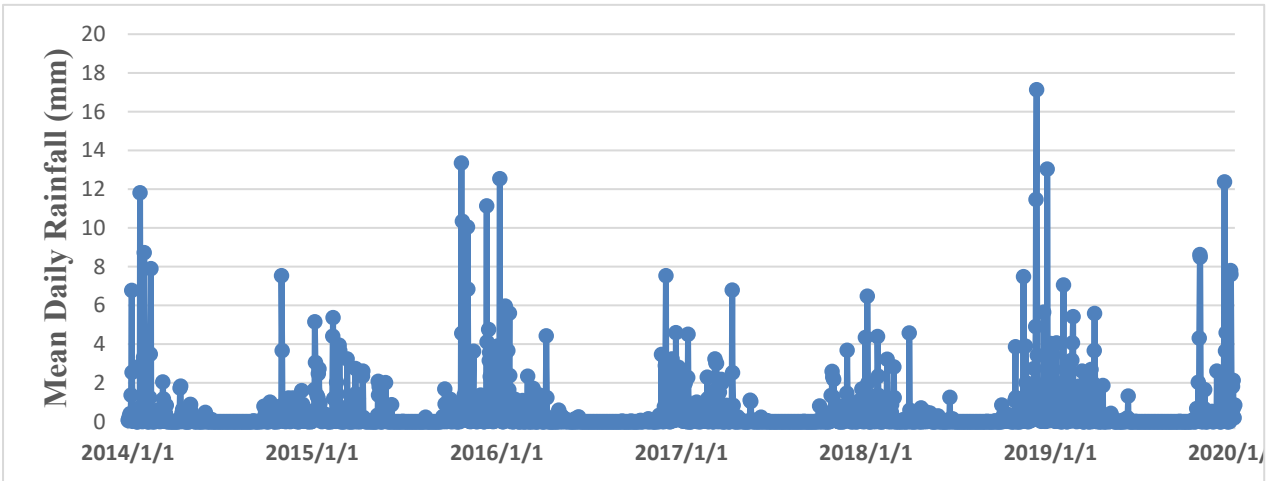

Figure 4. Sample of the downloaded data from the GIOVANNI-NASA website.

These data were then processed to obtain the total monthly rainfall (mm) over time. Thereafter, we get the maximum rainfall for the whole series (1979–2020). Table 1 shows the statistical description of theses rainfall records. We found that the study area experienced maximum and minimum precipitation of 319 and 2.77 mm/year, respectively, where the maximum rainfall ranged from 35 mm to 319 mm, occurring in 2017 and 2018. The minimum records ranged from 2.77 to 7.03, mostly in 2000 and 2001. Figure 5 shows the rainfall trend for the selected stations from 1979 to 2020. For the first period, from 1979 to 2014, rainfall values ranged from 2 mm to 50 mm, exceeding the mean, and others fell below it, due to topography, humidity, and temperature changes, where the variation is almost in a cyclic action. As for the last decade, there was a huge change in annual rainfall due to climate change, as the rainfall exceeded 300 mm. Accordingly, a decadal analysis was conducted to study the noticeable change in the rainfall trend.

Table 1. Statistical description of the rainfall records.

Stations	Max	Min	Average	SD	Variance
1	47.3	3.18	11.371429	8.5877481	73.7494174
2	54.6	2.77	12.692619	9.8558533	97.1378442
3	35.8	2.58	11.30119	7.7171394	59.55424
4	39.8	2.79	11.168095	7.7084225	59.4197768
5	44.2	3.38	11.537619	7.6467413	58.4726527
6	99.7	5.26	14.874048	15.170064	230.130854
7	98.8	5.13	15.166429	15.04813	226.446224
8	106	4.28	15.838333	16.133449	260.288161
9	100	4.47	15.189286	15.180393	230.444329
10	74.4	5.38	15.200238	12.852486	165.186407
11	71.8	5.14	15.112619	12.605148	158.889766
12	73.4	5.85	15.676429	12.469051	155.477243
13	135	4.59	18.96619	20.114672	404.600039
14	319	6.49	26.921905	49.689499	2469.04631
15	289	6.22	26.043095	44.515051	1981.58974
16	187	7.03	21.587381	27.81516	773.683147
17	149	6.61	21.760238	24.42936	596.793632

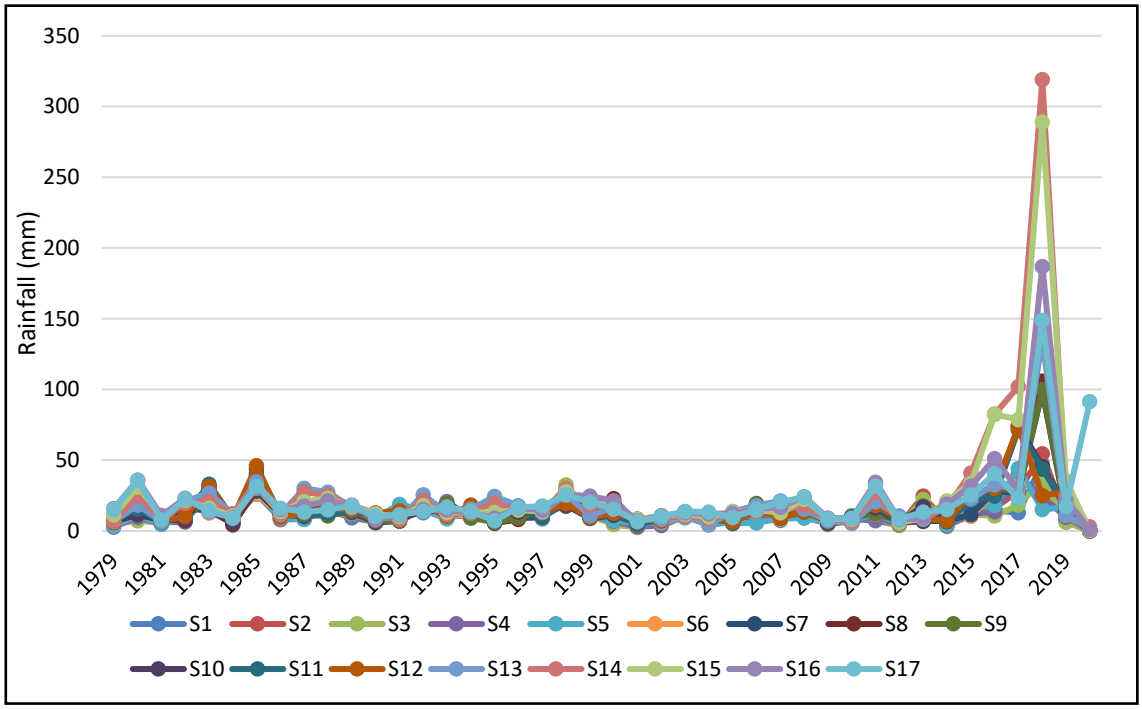

Figure 5. Rainfall trend for the selected stations.

2.3.5. Evapotranspiration data

The data for the average evapotranspiration rate per month for the Northwest Coast was downloaded from the "AQUASTAT Climate Information Tool" for 2009 to 2020, as shown on Figure 6 [45]. The data emphasizes significant interannual fluctuations and a distinct upward trend following 2017. The minimum value was recorded in 2011 at approximately 143 mm/month, whereas the maximum was noted in 2019 at around 162 mm/month, reflecting an increase in atmospheric water demand. Starting from 2018, evapotranspiration consistently surpassed 155 mm/month, indicating the potential impact of rising temperatures and extended dry weather associated with climate change. This increasing trend in evapotranspiration could lead to increased water stress, reduced soil moisture, and increased irrigation requirements, highlighting the need for incorporating evapotranspiration dynamics into water resource and flood management strategies.

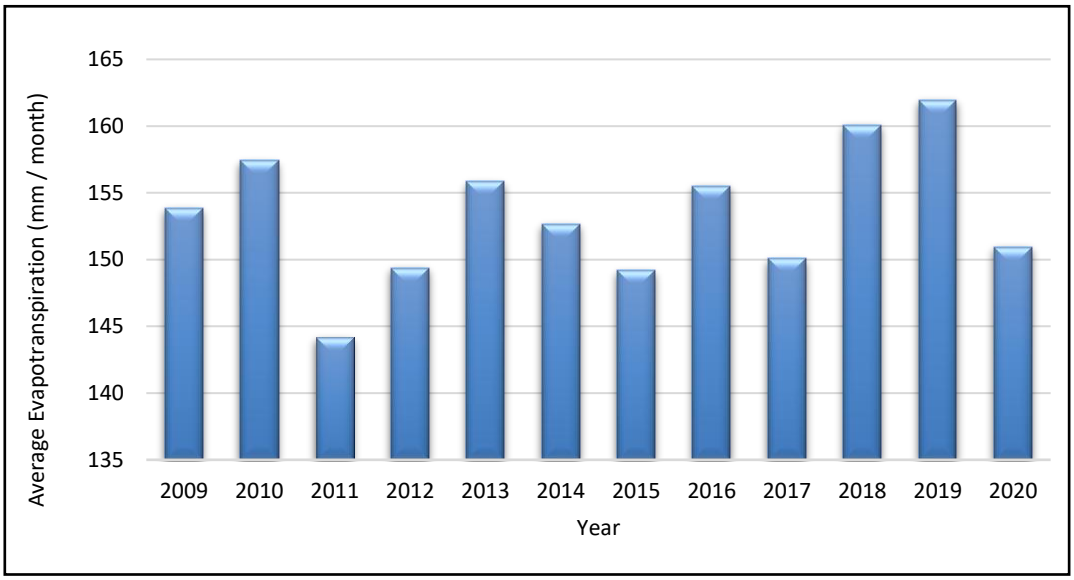

Figure 6. Average evapotranspiration mm/month on the Northwest Coast.

3. Results

3.1. Morphological results for the study area

A Digital Elevation Model (DEM) with 30 m resolution was utilized to perform the delineation and extract basin characteristics using WMS and ArcGIS 10.8 [46]. The delineation process included defining 45 morphometric parameters, including the flow paths, drainage networks, reach lengths, and basin boundaries. We focused on basins with an area greater than 500 km², leading to the selection and analysis of seven drainage basins, as shown in figure 7.

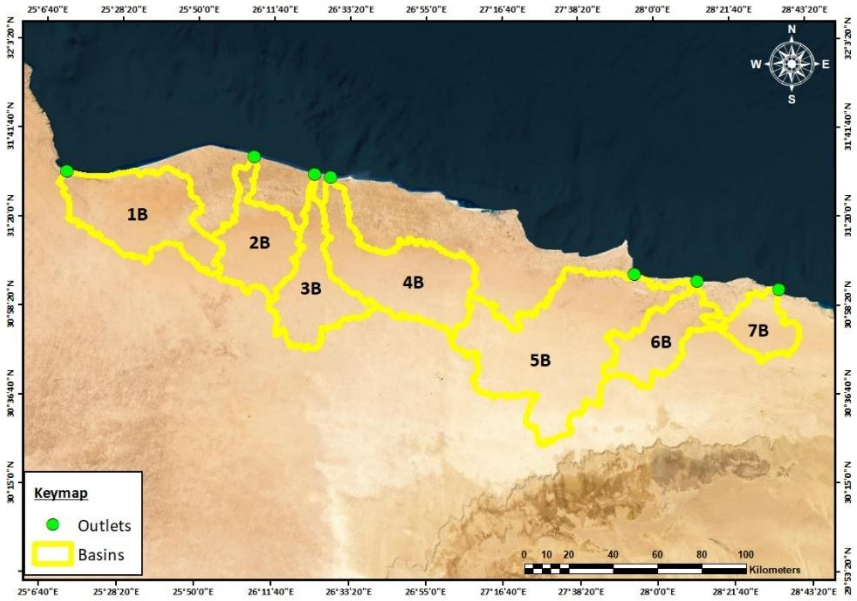

Figure 7. The boundaries of the selected basins.

The delineation began with determining the flow accumulation through the slope analysis of the DEM. Thereafter, flow direction could be identified, followed by stream order identification, to obtain the basin boundaries with an identified outlet point for each basin. Figure 8 shows the DEM for the seven basins; it appears that the area levels are almost flat ranged, from a few meters at the coast, to about 240 m at the highest areas.

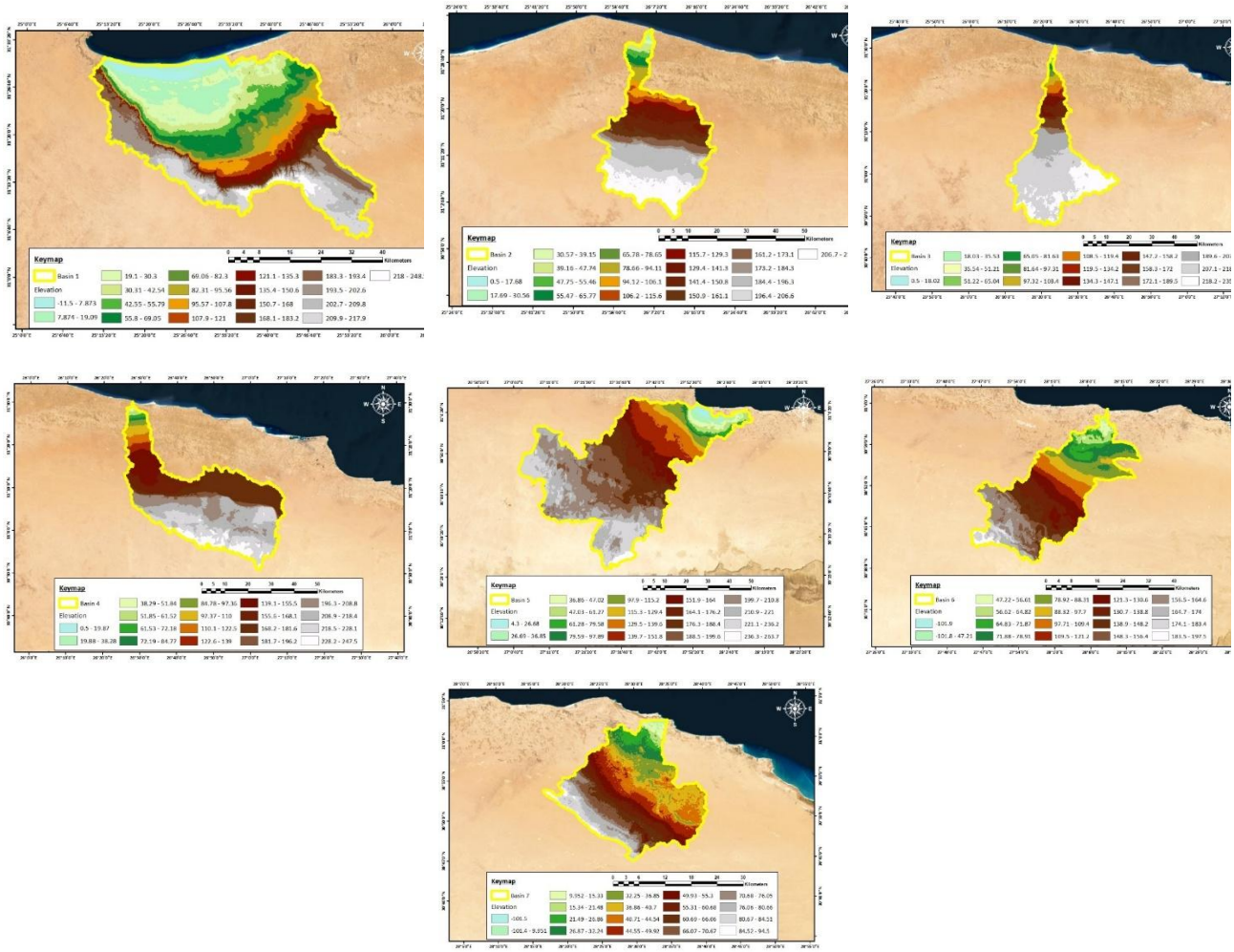

Figure 8. The digital elevation model results for each selected basin.

Figure 9 represents the flow direction and shows that the central and southern parts of the basin exhibit more complex flow patterns, likely influenced by varying topography of hills, resulting in diversified runoff pathways. In contrast, the northern sections of the basin, especially those adjacent to the coastal boundary, show more uniform flow convergence, highlighting these areas as potential drainage outlets and areas prone to surface water accumulation.

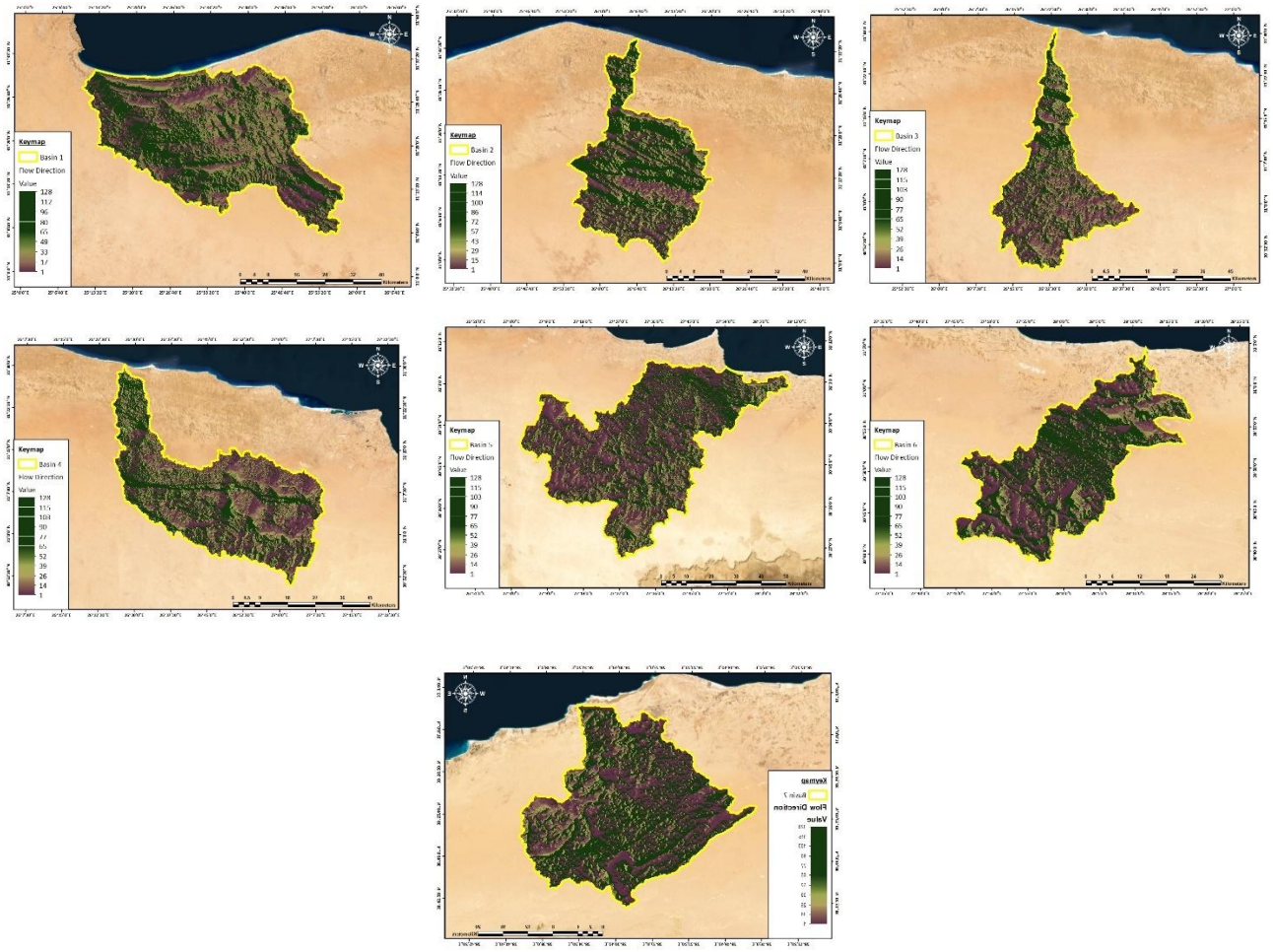

Figure 9. The flow direction for selected basins.

Figure 10 shows the slope of each subbasin, which slope toward the coast. It also shows that most of the subbasins are characterized by gentle to moderate slopes, which influence surface runoff dynamics and infiltration potential, while steeper slopes primarily concentrated in the southern and southeastern regions promote rapid runoff and increase the risk of soil erosion and flash flooding.

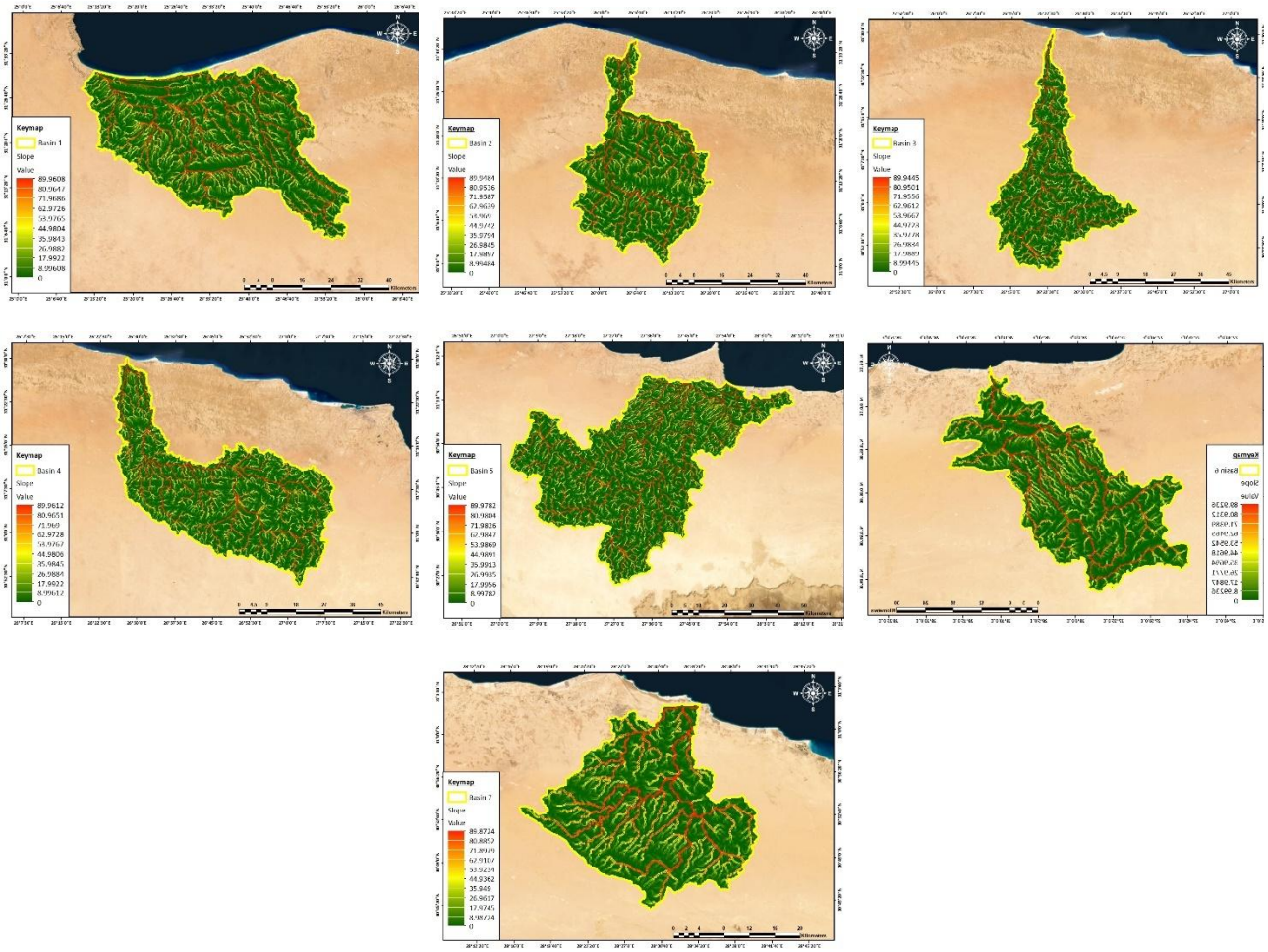

Figure 10. The slope for each selected basin.

Figure 12 presents the flow distance for the subbasins, showing the spatial variation in flow path lengths from each grid cell to the basin outlet, reflecting the topographic control on surface water movement, basin morphology, slope, and drainage network configuration that influence the hydrological response. Flow distance is vital for assessing time of concentration, modeling hydrograph timing, and identifying areas where floodwaters may accumulate or be delayed, thereby informing flood hazard assessment and mitigation planning.

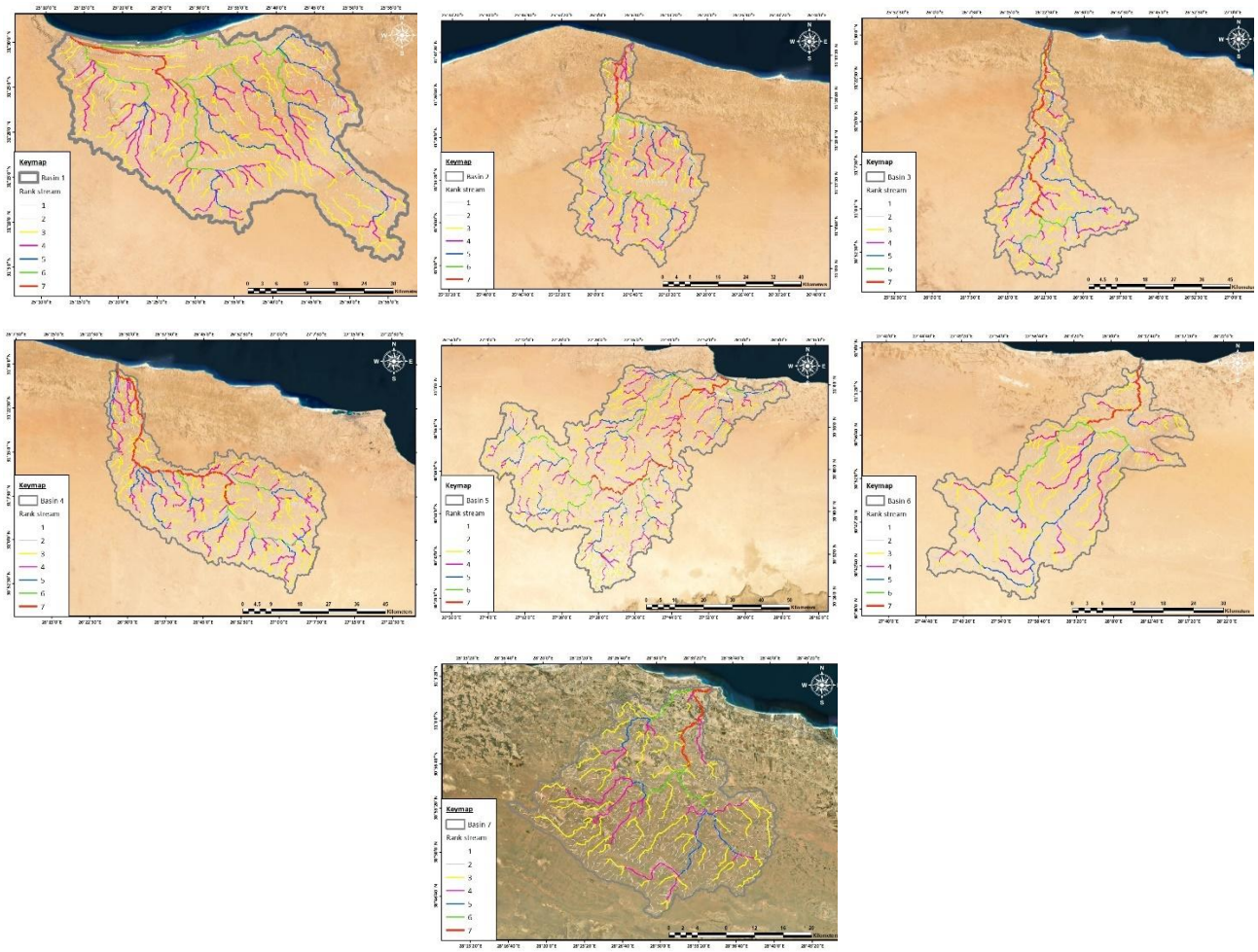

Figure 11. The stream orders for each selected basin.

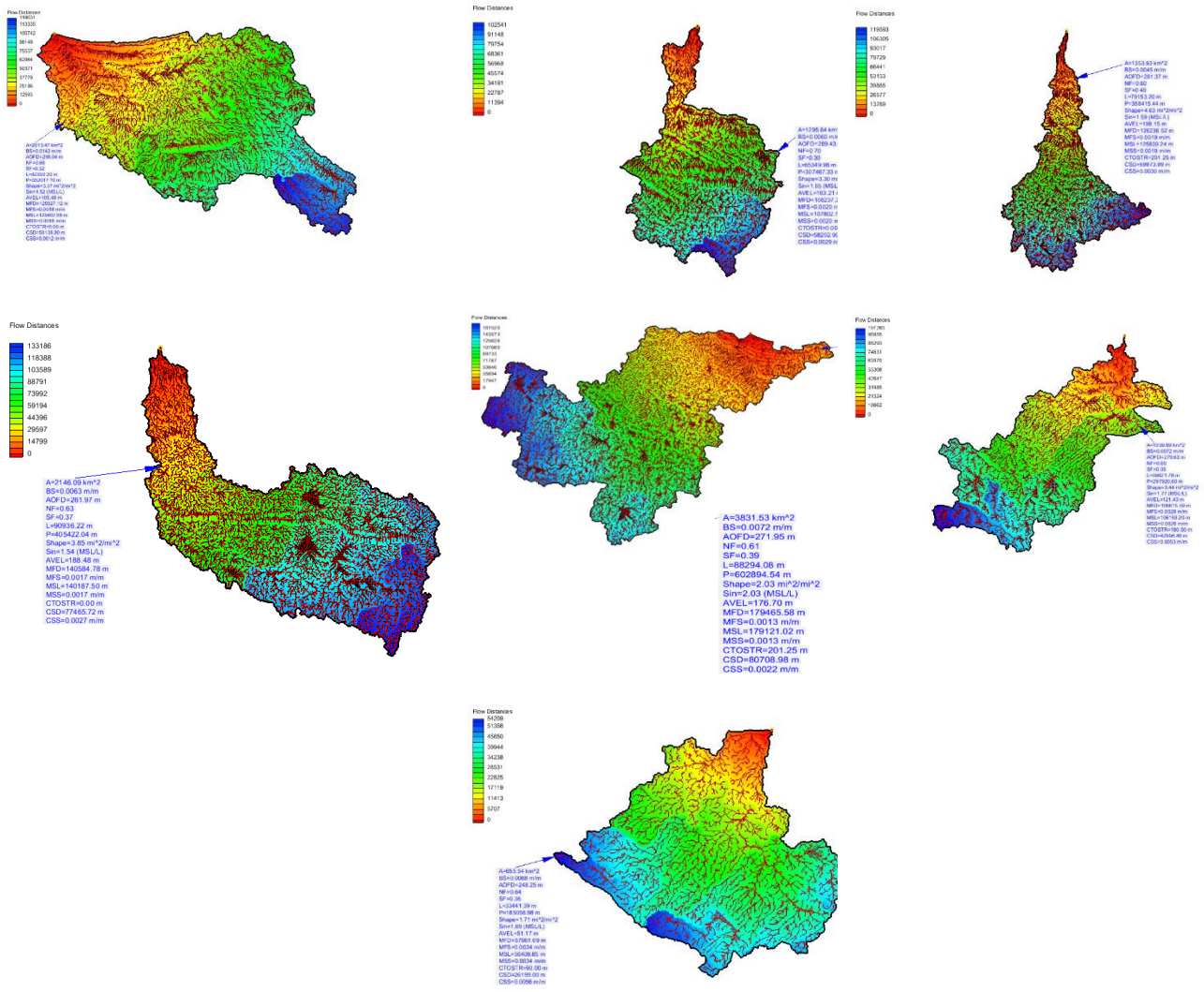

Figure 12. The flow distance for the subbasins and the major morphological parameters.

The extracted morphometric parameters were systematically classified into four major categories: Basin geometry, drainage network characteristics, relief analysis, and texture analysis. These parameters were quantified and expressed through a set of statistical parameters, as detailed in Table 2. The computed results for each category are presented in Tables 3 through 7, providing insights into the basin's hydrological behavior, topographic structure, and drainage efficiency.

Table 2. Formulas of morphometric parameters.

Basin Geometry			
S.no.	Parameters	Formula	Reference
1	Basin Width	$W_b = A_b / L_b$	[47]
2	Basin Relative Perimeter	$P_r = A_b/P$	[48]
3	Length Area Relation	$L_{ar} = 1.4 * A_b^{0.6}$	[49]
4	Lemniscate	$K = L_b^2 * \pi/4A_b$	[50]
5	Form Factor Ratio	$F_f = A_b / L_b^2$	[47]
6	Elongation Ratio	$R_e = \frac{2 * \sqrt{\frac{A_b}{\pi}}}{L_b}$	[48]
7	Circularity Ratio	$R_c = 4 * \pi * A_b/P^2$	[51]
8	Circularity Ration	$R_{cn} = A_b/P$	[52]
9	Topographic Texture Ratio	$T = N_u/P$	[53]
10	Compactness Coefficient	$C_c = 0.2841 * P/\sqrt{A_b}$	[47]
11	Basin shape index	$I_{sh} = 1.27 * A_b/L_b^2$	[54]
12	Compactness ratio	$SH = P_r/2 * \sqrt{\frac{A_b}{\pi}}$	[47]
Drainage Network			
S.no.	Parameters	Formula	Reference
1	Stream number	$N_u = N_1 + N_2 + \cdots N_n$	[15]
2	Stream Length	$L_u = L_1 + L_2 + \cdots L_n$	[55]
3	Stream Length ratio	$L_{ur} = L_u/L_{u-1}$	[55]
4	Bifurcation Ratio	$R_b = N_u / N_{u+1}$	[15]
5	Rho Coefficient	$\rho = L_{ur} / R_b$	[15]
Relief Characterizes			
S.no.	Parameters	Formula	Reference
1	Maximum Elevation of the Basin (Z) Minimum Elevation of the Basin (z)	Elevation of highest summit. Measured directly using WMS software Analysis using DEM	[55]
2	Total Basin Relief	$H = Z - z$	[55]
3	Relief Ratio	$R_{hl} = H/ L_b$	[48]
4	Absolute Relief	$R_a = Z$	[56]
5	Relative Relief Ratio	$R_{hp} = \frac{H * 1000}{P}$	[56]
6	Dissection Index	$D_{is} = H/R_a$	[57]
7	Ruggedness Number	$R_n = D_d * H/1000$	[56]
8	Melton Ruggedness Number	$MR_n = H/\sqrt{A_b}$	[58]
Drainage Texture			

S.no.	Parameters	Formula	Reference
1	Stream Frequency	$F_s = N_u * A_b$	[47]
2	Drainage density	$D_d = L_u/A_b$	[47]
3	Constant of Channel Maintenance	$C = 1/D_d$	[48]
4	Drainage Intensity	$D_i = F_s/D_d$	[59]
5	Infiltration Number	$I_f = F_s * D_d$	[59]

The morphometric parameters shown in Table 2 were selected based on their influence on flood generation, runoff concentration, and basin susceptibility. Basin geometry parameters, such as basin width, elongation ratio, and form factor, determine the potential for flow convergence and the time of concentration. Drainage network characteristics, such as stream number, bifurcation ratio, and stream length, control how quickly runoff is routed through the basin. Relief parameters, such as, maximum elevation, basin relief, and dissection index, influence the energy available for runoff movement and the potential for flow accumulation in low-lying areas. Drainage texture parameters, such as drainage density, stream frequency, and infiltration number, govern infiltration capacity and the speed of runoff concentration, which are particularly critical in arid coastal basins where vegetation is sparse and rainfall is intense. Collectively, these parameters provide a physically grounded framework for assessing flood susceptibility and enable the analysis to be reproducible in similar arid coastal environments.

Table 3. Major basin parameters.

No. of basin	Name of basin	Area (A_b)	Length (L_b)	Perimeter (P)
1	Wadi El-Qireisa	2013.47	82350.2	352017.7
2	Wadi El-Harika	1295.64	65349.98	307467.33
3	Wadi El-Shammas	1353.93	79153.2	358415.44
4	Wadi Marzug	2146.09	90936.22	405422.04
5	Wadi Khreisa	3831.53	88294.08	602894.54
6	Wadi Baghoush	1039.89	59821.78	297920.6
7	Wadi Makman	655.54	33441.39	185058.98

Table 3 shows the major basin parameters of the seven subbasins, revealing significant variations in their spatial and geometric characteristics. Wadi Khreisa (Basin 5), being the largest basin with an area of 3831.53 km² and the widest regarding perimeter, indicates a complex and wide drainage area. In contrast, Wadi Makman (Basin 7) is the smallest basin with an area of 655.54 km2 and is the most compact, reflecting a simpler hydrological structure. Basins such as Wadi El-Qireisa and Wadi Marzug also exhibit substantial areas and lengths, suggesting their importance in regional runoff dynamics. Variations in perimeter-to-area ratios across the basins highlight differences in shape and boundary complexity, which influence hydrological behavior, runoff concentration, and flood potential.

Table 4. Geometric parameters.

No.	P_r	W_b	L_{ar}	K	F_f	SH	I_{sh}	R_e	R_c	R_{cn}	T	C_c
1	5719.8	24450.1	535174.2	2.64395	0.29690	0.03596	0.377067	0.614997	0.204186	0.016248	0.03049	2.22876
2	4213.9	19826.2	410788.9	2.58747	0.30338	0.03303	0.385298	0.621672	0.172225	0.013705	0.02349	2.42677
3	3777.5	17105.2	421779.8	3.63253	0.21610	0.02896	0.274449	0.524680	0.132444	0.010539	0.01988	2.76732
4	5293.5	23599.9	556053.8	3.02479	0.25952	0.03224	0.329592	0.574979	0.164075	0.013056	0.02698	2.48631
5	6355.2	43395.1	787320.2	1.59720	0.49148	0.02897	0.624184	0.791261	0.132464	0.010541	0.03355	2.76711
6	3490.5	17383.1	360014.9	2.70147	0.29058	0.03054	0.369039	0.608414	0.147230	0.011716	0.01848	2.62469
7	3542.3	19602.7	272952.8	1.33918	0.58617	0.03903	0.744447	0.864132	0.240541	0.019141	0.01695	2.05344

Table 4 shows the geometric parameters for the seven subbasins, revealing significant variability in basin geometry and drainage characteristics. It shows that Wadi Makman (Basin 7) exhibits the highest form factor Ff = 0.58617 and the lowest elongation ratio with K = 1.34, indicating a compact, circular shape associated with rapid runoff and higher flood potential. In contrast, Wadi El-Shammas (Basin 3) has a low form factor of Ff = 0.21610 and high elongation ratio of K = 3.63, reflecting an elongated shape that promotes delayed runoff and lower peak flows. Compactness coefficient values further differentiate drainage efficiency, as Wadi Makman displays the most efficient shape with Cc = 2.05, while basins like Wadi Khreisa (Basin 5) and Wadi El-Shammas (Basin 3) exhibit more elongated and less efficient forms with Cc = 2.76.

Table 5. Drainage parameters.

No.	N_u	L_u	L_{ur}	R_b	ρ
1	10734	2940193	1.533730409	1.451169767	1.056892477
2	7223	3328539	1.561040429	1.540989455	1.013011753
3	7124	2863596	1.519244278	1.460742088	1.040049637
4	10939	3123988	1.37353622	1.374083907	0.999601417
5	20226	3048142	1.35574604	1.383033635	0.980269753
6	5505	2586183	1.505252679	1.444481281	1.042071433
7	3136	1461615	1.454529818	1.427084274	1.019231902

Table 5 shows the drainage parameters, revealing variations in stream development and hydrological responses among the seven sub-basins. These parameters are vital for understanding runoff behavior, erosion risk, flood hazard, and physical susceptibility for the study area. Wadi Khreisa (Basin 5) has the highest stream frequency with Nu = 20,226 despite a moderate total stream length, indicating a highly divided and reactive landscape, while Wadi Makman (Basin 7) has the lowest stream development due to its smaller size. The length of the overland flow (Lur) ranges from 1.35 to 1.56, with shorter flow paths in larger basins, suggesting quicker runoff concentration. Bifurcation ratios (Rb) fall within a moderate range from 1.37 to 1.54, indicating relatively stable and mature drainage systems with minimal structural distortion. Drainage density (ρ) varies slightly among basins from 0.98 to 1.06, with higher values in Wadis El-Qireisa (Basin 1) and El-Shammas (Basin 3), reflecting more efficient surface drainage and lower infiltration potential.

Table 6. Relief parameters.

No.	Z	z	H	R_{hl}	R_n	R_a	R_{hp}	D_{is}	MR_n
1	248.5	-11.5	260	0.00315	0.000379	248.5	0.07385	1.04627	0.00579
2	219.5	0.5	219	0.00335	0.000562	219.5	0.07122	0.99772	0.00608
3	235.6	0.5	235.1	0.00297	0.000497	235.6	0.06559	0.99787	0.00638
4	247.5	0.5	24	0.00271	0.000359	247.5	0.06092	0.99797	0.00533
5	263.8	4.3	259.5	0.00293	0.000206	263.8	0.04304	0.98369	0.00419
6	197.5	-101.9	299.4	0.00501	0.000744	197.5	0.10049	1.51594	0.00928
7	94.5	-101.5	196	0.00586	0.000437	94.5	0.10591	2.07407	0.00765

Table 6 shows the relief parameters, offering insight into the vertical characteristics and erosion potential of the seven basins. Basin altitude (Ba) ranges from 94.5 m to 263.8 m, while basin relief (H) varies notably, with Wadi Baghoush (Basin 6) and Wadi Makman (Basin 7) showing the highest relief values of 299.4 m and 196 m, respectively, reflecting steep terrain. These subbasins also record the highest relative relief (Rhp) and dissection index (Dis), indicating intense vertical dissection and pronounced topographic variation, which enhance erosion potential and rapid runoff. On the other hand, Wadi Khreisa (Basin 5) displays low Rhp and Dis, suggesting a more subdued landscape. The ruggedness number (Rn) and Melton ruggedness ratio (MRn) are highest in Basins 6 and 7, confirming their steep and erosively active nature. The gradient ratios (Rhl and Ra) are also elevated in these two basins, reinforcing the interpretation of strong terrain gradients.

Table 7. Drainage texture.

Ba	D_d	F_s	C	D_i	I_f
1	0.00146	5.331E-06	684.808	0.00365	7.784E-09
2	0.00256	5.574E-06	389.251	0.00217	1.432E-08
3	0.00211	5.261E-06	472.807	0.00248	1.112E-08
4	0.00145	5.097E-06	686.971	0.00350	7.419E-09
5	0.00079	5.278E-06	1257.005	0.00663	4.199E-09
6	0.00248	5.293E-06	402.094	0.00212	1.316E-08
7	0.00222	4.783E-06	448.503	0.00214	1.066E-08

Table 7 shows the drainage texture describing the efficiency of surface runoff, infiltration, and drainage development across the basins. Wadi Khreisa (Basin 5) exhibits the lowest drainage density (Dd) with a value of 0.00079, and the highest constant of channel maintenance with C = 1257.005, indicating a well-drained basin with low surface runoff and high infiltration potential. In contrast, Wadis El-Harika (Basin 2), Baghoush (Basin 6), and Makman (Basin 7) show relatively higher drainage densities, Dd ≥0.0022, suggesting more developed drainage systems and greater runoff generation. The drainage intensity (Di) is highest in Basin 5, pointing to a low degree of stream development relative to drainage density. Additionally, infiltration number (If) values are highest in Basins 2 and 6, implying limited infiltration and increased surface flow, which may elevate flood risk.

3.2. Rainfall analysis

Figure 13 presents the maximum rainfall recorded at selected stations along the West North Coast. The time series data were categorized into four periods: 1979–1988, 1989–1998, 1999–2008, and 2009–2020. Regarding temporal variation, the analysis indicates that the 2009–2020 period consistently exhibits the highest rainfall across nearly all stations, whereas the preceding decades show relatively similar rainfall values with minor fluctuations. In terms of spatial variation, stations S14, S15, S16, and S17 recorded significantly higher rainfall during 2009–2020 compared to earlier decades. This suggests that these locations may be more susceptible to extreme weather events or shifting climate patterns, potentially increasing the risk of flooding. Consequently, these findings have implications for drainage system design and coastal flood management.

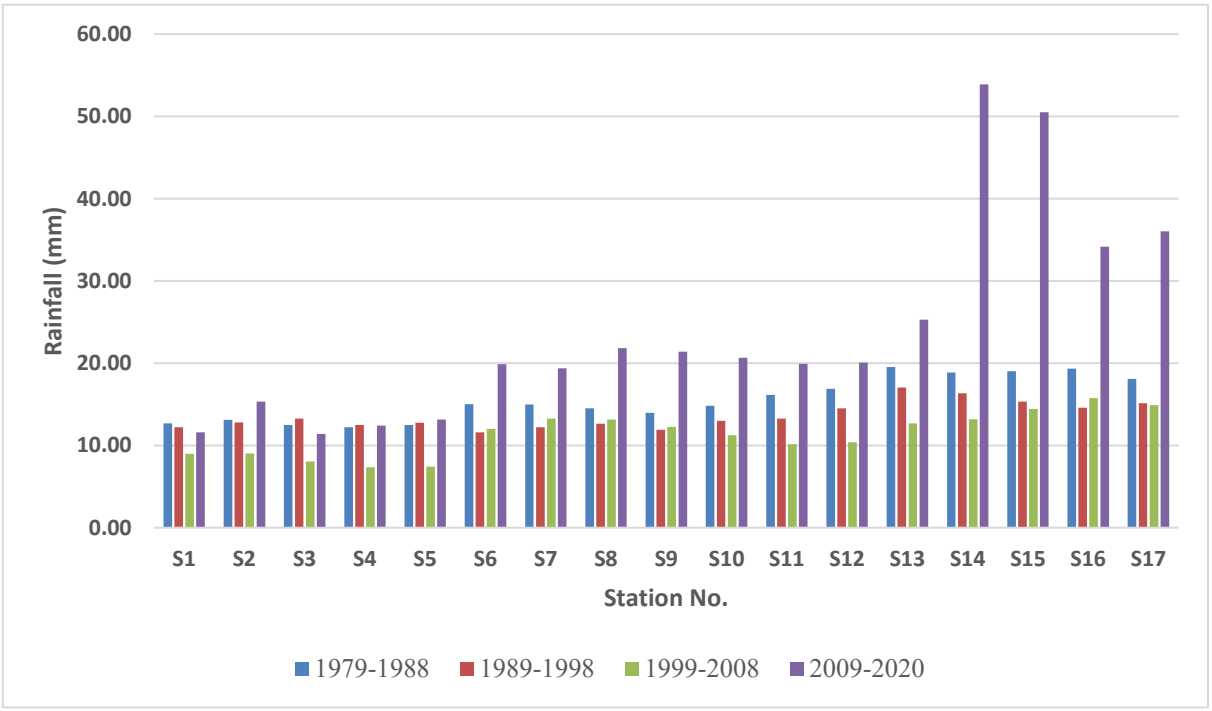

Figure 13. The decadal rainfall analysis on the Northwest Coast.

To evaluate the flood risk, the corresponding rainfall values for 100-year return period estimation at 5% confidence level was calculated using HYFRAN-PLUS software. This 100-year return period was selected because it was the more significant from a hydrological perspective and managed the extremes effectively in arid and semi-arid regions, which receive infrequent but intense rainfall leading to flash floods. The rainfall frequency analysis was conducted using five statistical probability distribution functions, which are Gumbel, Weibull, Gamma, Normal, and Log-Normal. For each station, the best fitting distribution was determined using goodness-of-fit criteria to ensure reliability and precision for the estimation. This was done for the rainfall data gathered from the stations in the seven basins under study. As presented in Table 11, the results include the selected probability distribution method for each station. Figure 14 provides a sample output from HYFRAN-PLUS. Along with the extreme value analysis, decadal rainfall data were analyzed to capture the temporal changes and the impact of climate change on the intensity and frequency of rainfall.

Table 8. The frequency analysis results of the rainfall stations for a 100-year return period.

Rain gauges	Precipitation (mm)	Method
S1	36.7	Weibull
S2	42	Weibull
S3	34.6	Weibull
S4	34.5	Weibull
S5	202	Gumbel
S6	118.3	Log Normal
S7	54.2	Gamma
S8	59	Gamma
S9	55.3	Gamma
S10	53.3	Gamma
S11	271	Gumbel
S12	51.5	Gamma
S13	78.9	Log Normal
S14	108.7	Log Normal
S15	159	Log Normal
S16	88.98	Log Normal
S17	71	Log Normal

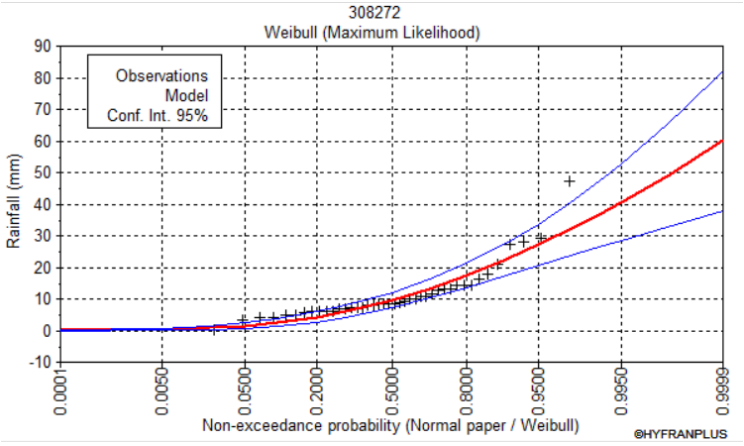

Figure 14. Average evapotranspiration rate/month for one station on the Northwest Coast.

The spatial distribution of rainfall across the seven basins was determined using the annual average rainfall recorded at all rainfall stations and was analyzed through the Thiessen polygon method. In this study, the Thiessen polygon technique was implemented in WMS software to estimate peak flood discharge by incorporating gauge weights.

3.3. Hydrological analysis

The Soil Conservation Service (SCS) Curve Number (CN) method was utilized within HEC-HMS to estimate the runoff for each subbasin. The runoff was calculated for the 100-year return period and the decade with the highest recorded rainfall (2009–2020). Figure 15 presents the HEC-HMS, where

the resultant hydrograph shapes show a short concentration time, implying that rainfall is quickly converted into runoff, likely due to steep slopes, low infiltration capacity, and sparse vegetation, which are typical in arid regions.

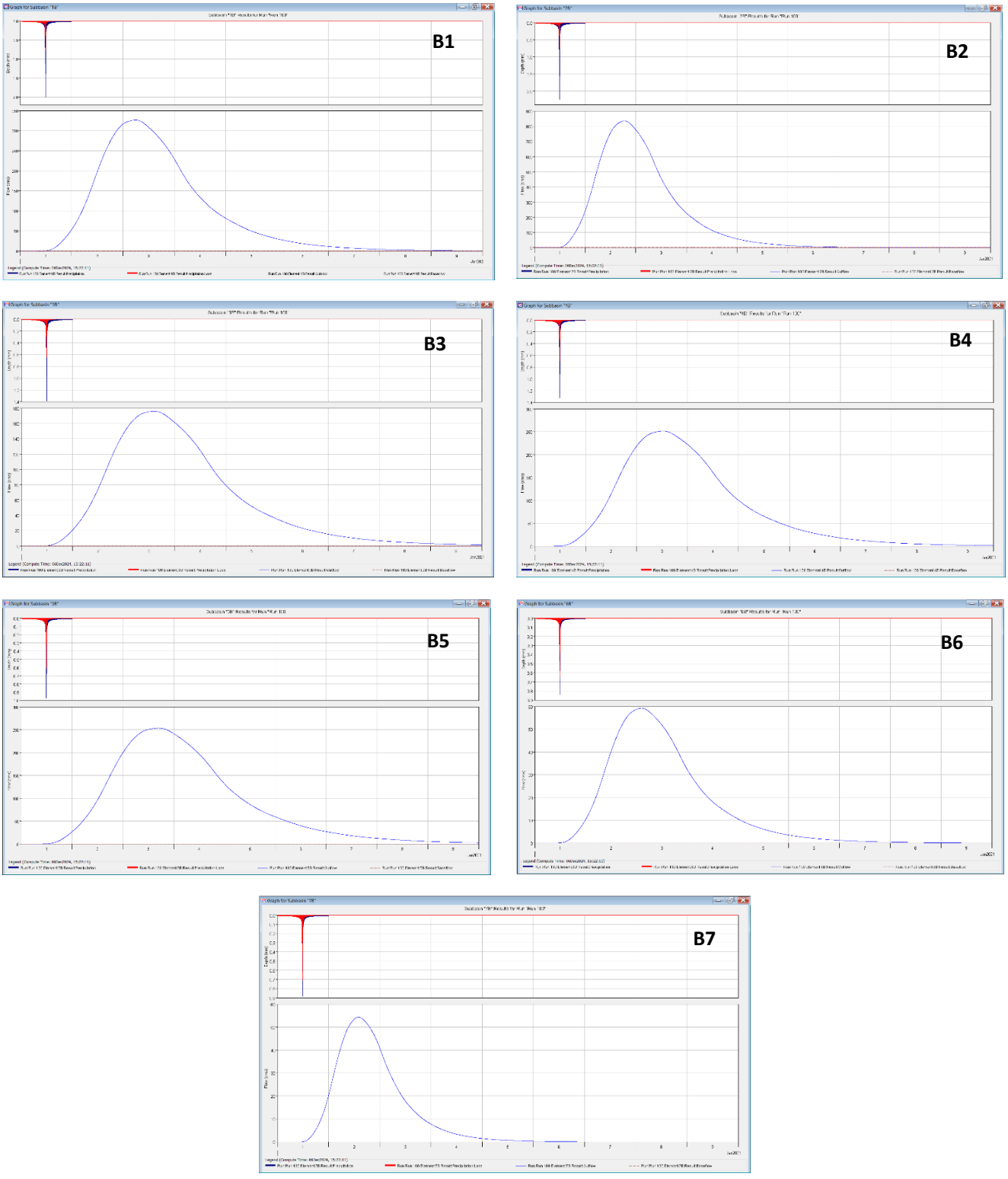

Figure 15. HEC-HMS results for the seven subbasins for a 100-year return period.

Figure 16 illustrates the simulated hydrographs for all seven sub-basins under a 100 year return period rainfall event. The results reveal significant variability in hydrological response across the study area. Notably, Basin 2 exhibits the highest peak discharge, reaching approximately 800 m^3/s, accompanied by a maximum flow depth exceeding 2 meters, indicating a high potential for flash flooding. This response may be attributed to its larger drainage area, steeper slopes, or more efficient flow accumulation network. Conversely, Basin 7 demonstrates the lowest peak flow, estimated at around 55 m^3/s, with a corresponding flow depth below 0.9 meters, reflecting its smaller basin area and potentially lower runoff generation capacity. These variations underscore the importance of basin-specific flood risk assessments and the need for tailored mitigation strategies based on individual basin characteristics.

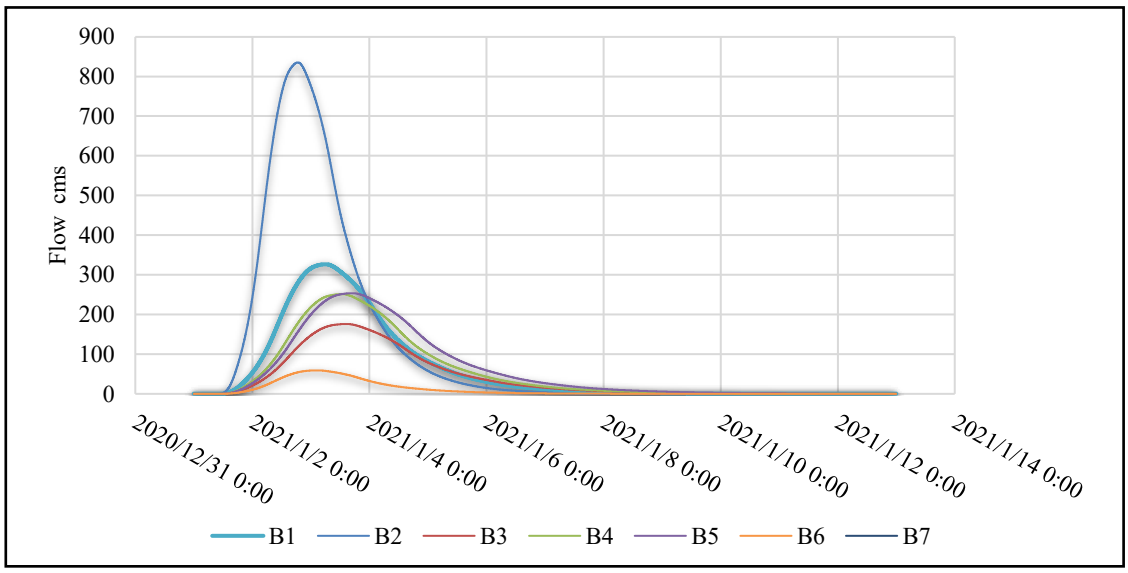

Figure 16. Runoff hydrograph of a 100-year return period for the seven subbasins.

For the decadal analysis, Figures 17 (a-d) illustrate the decadal runoff hydrographs for each basin within the study area. The findings indicate that the final decade of the study period (2009–2020), Figure 5-d, exhibits the highest runoff hydrograph, directly attributed to the increased rainfall during this period. The peak runoff values range from 187 m^3/s in Basin 2 to 2.2 m^3/s in Basin 7, aligning with the runoff characteristics observed for the 100-year return period. Additionally, Basins 1, 3, 4, and 5 demonstrate moderate peak runoff values of 45 m^3/s, 22 m^3/s, 35 m^3/s, and 18 m^3/s, respectively. In contrast, Basins 6 and 7 record the lowest peak discharge, with values of 2.5 m^3/s and 2.2 m^3/s, respectively. On the other hand, the third decade of 1999–2008, Figures 17-b, exhibit the lowest runoffs for all basins, with a maximum value of 4 m3/s for basin 3 and a minimum value of 0.7 m3/s for basin 5.

3.4. Hydraulic analysis

The HEC-RAS model was employed to assess the extent of the flooded plain area and to produce flood inundation maps. Key input parameters, including streamlines and basin boundaries, were derived from WMS and HEC-HMS to estimate the expected floodwater depth. The analysis considered discharge corresponding to the decadal runoff for the period 2009–2020, as illustrated in Figure 18, as

well as the 100-year return period, depicted in Figure 19, showing the spatial variability of maximum water depth during a simulated flood event.

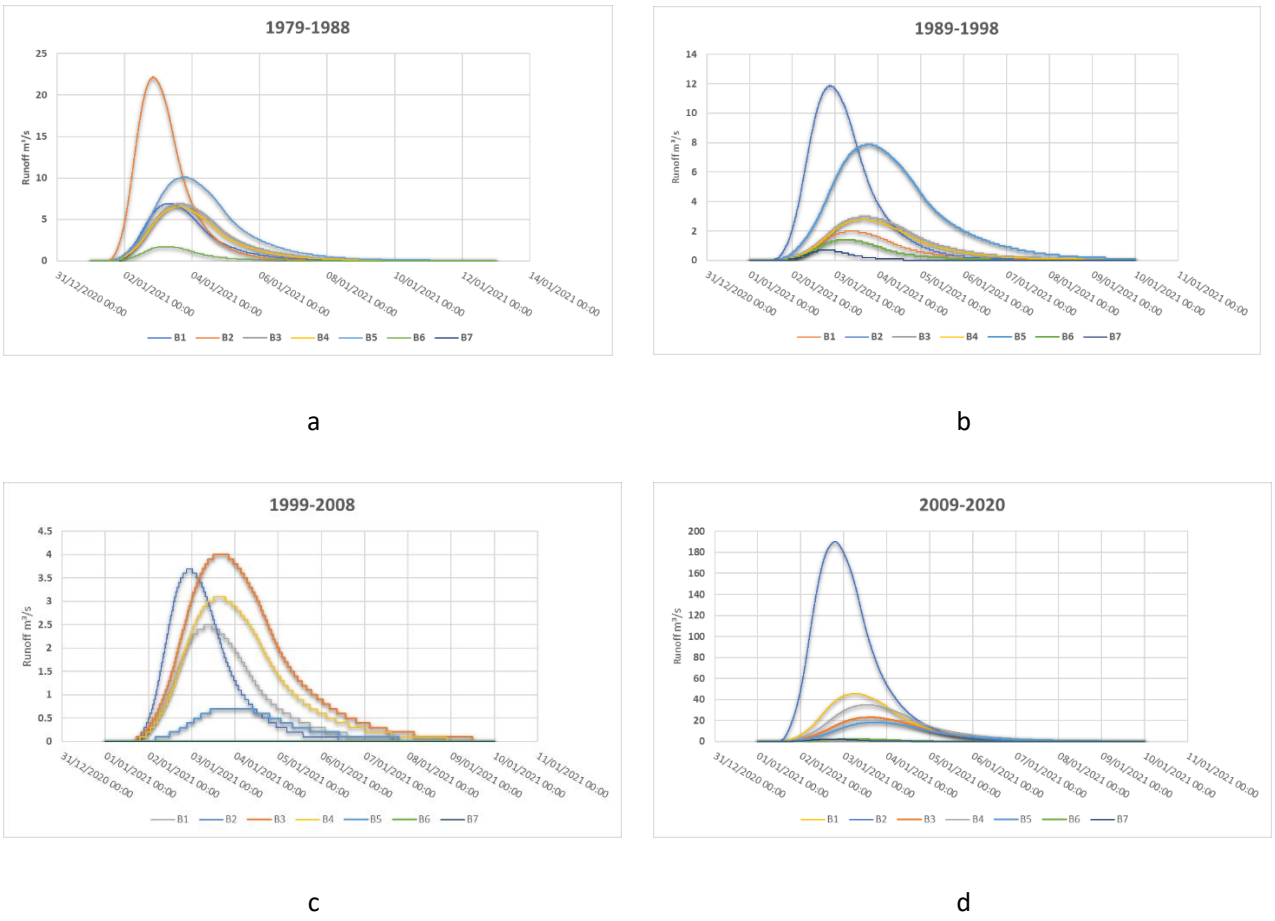

Figure 17. Runoff hydrograph of decadal analysis for all subbasins.

As for the decadal runoff for the period 2009–2020 presented in Figure 18, the results indicate that the maximum flood depth values range from about 1 meter for Basin 3 and Basin 4 to about 9 meters for Basin 1. The rest of the basins have moderate values of 3 and 6 m. For the 100-year return period presented in Figure 19, the results indicate that the maximum flood depth values range from about 3 m for Basin 3 to 30 m for Basin 5, where Basins 5, 6, and 7 experience the greatest flood depths, measuring 30 m, 13 m, and 17 m, respectively. Conversely, Basins 2, 3, and 4 exhibit the lowest flood depths, with values of 4 m, 3 m, and 3.2 m. The highest flow depths are mainly concentrated along the major drainage channels and confluence zones, reflecting areas of significant flood hazard, while shallower depths dominate the upper regions of the basins due to overland sheet flow across gently sloping terrain. The widespread inundation patterns suggest a rapid runoff response, characteristic of arid environments with low infiltration capacity, high runoff coefficients, and limited vegetation cover. The deepest zones near the coast indicate the accumulation of flood due to topographic flattening and limited drainage capacity. These patterns underscore the importance of micro-topography in flood routing and highlight the need for targeted flood risk assessments and infrastructure planning, particularly in areas with limited natural drainage outlets and potential urban expansion.

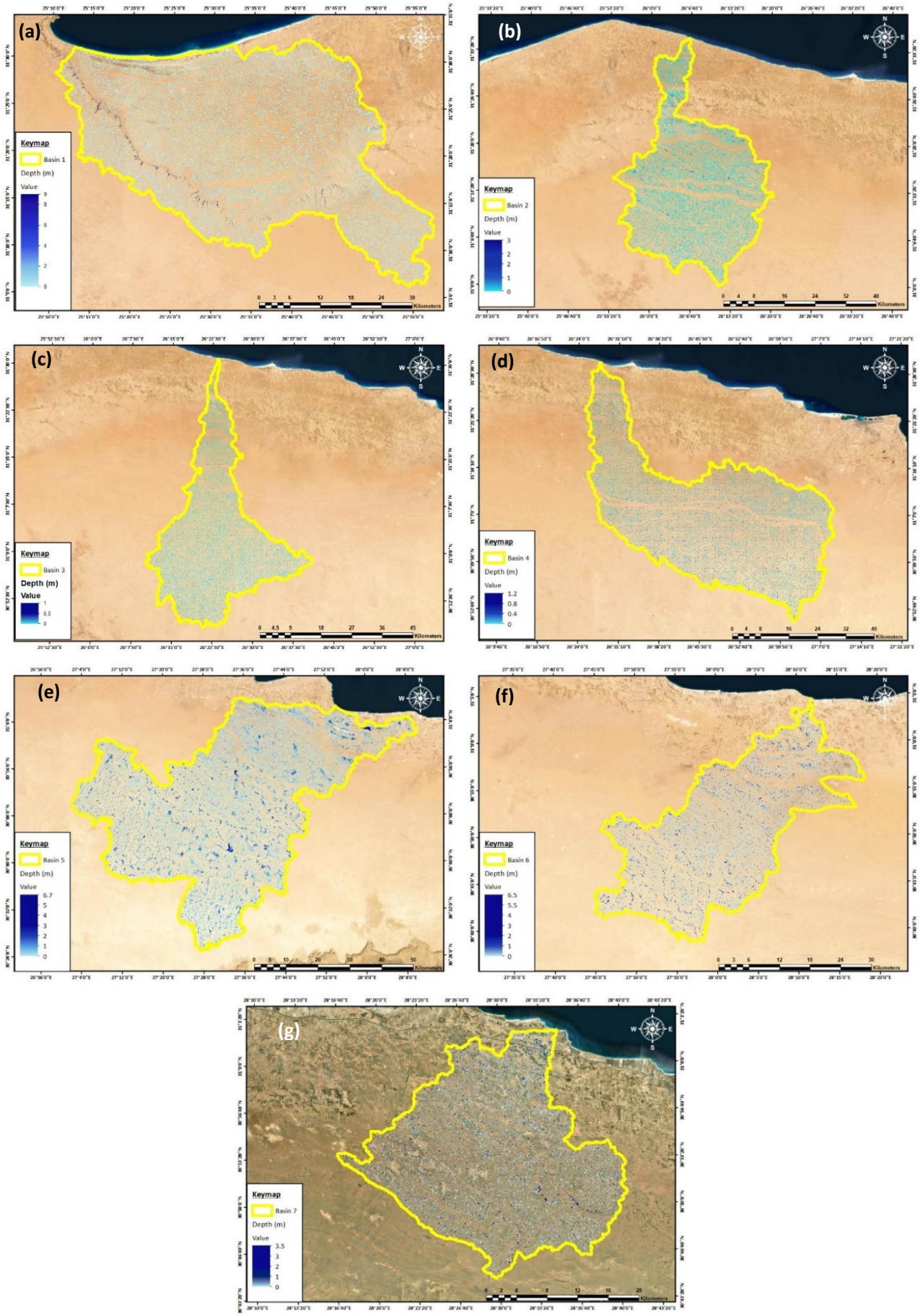
(a)
Keymap
Basin 1
Depth (m)
Value
(b)
Keymap
Basin 2
Depth (m)
Value
(c)
Keymap
Basin 3
Depth (m)
Value
(d)
Keymap
Basin 4
Depth (m)
Value
(e)
Keymap
Basin 5
Depth (m)
Value
(f)
Keymap
Basin 6
Depth (m)
Value
(g)
Keymap
Basin 7
Depth (m)
Value

Figure 18. Water depth for the highest decade of 2009–2020 for study area subbasins.

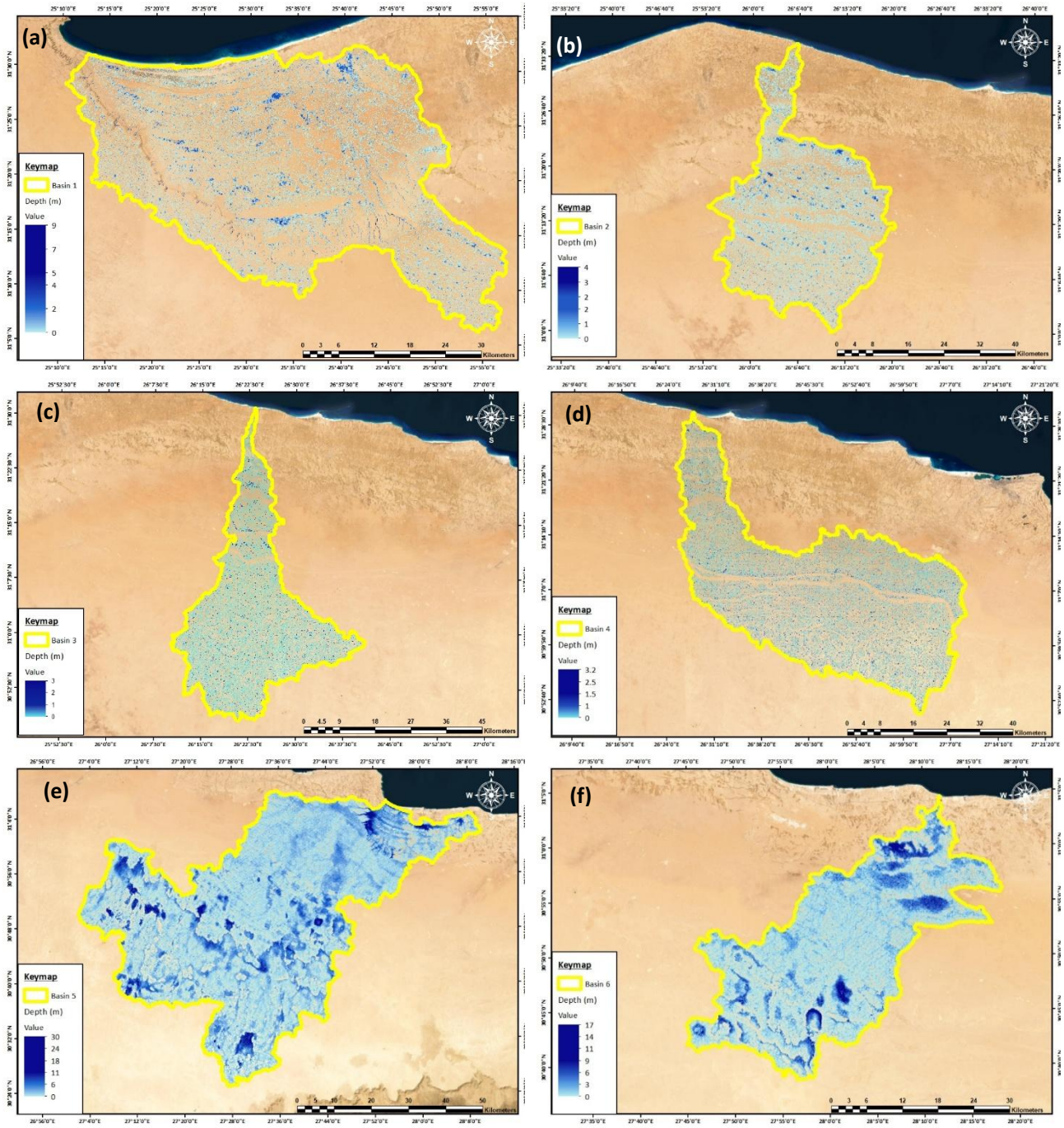

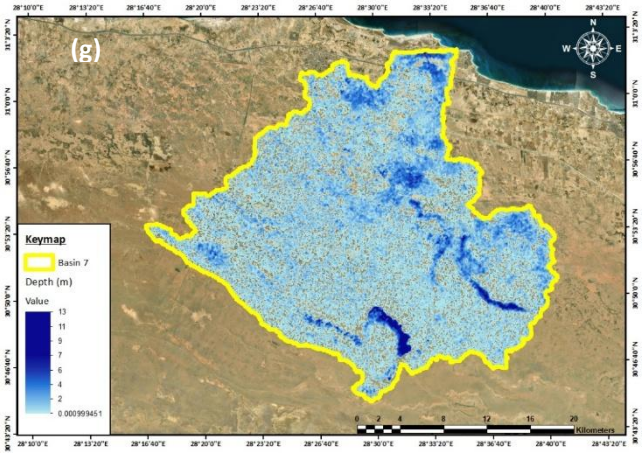

Figure 19. Water depth for the 100-year return period study area subbasins.

4. Discussion

4.1. Flood hazard analysis

The morphological parameters derived for each drainage basin vary in units, making direct comparison using conventional statistical methods challenging. To address this, a standardization process transforming the parameters into dimensionless values using weighted factors is employed. This facilitates meaningful comparison across basins. To explore the relationships between morphometric and hydrological characteristics, a statistical approach based on the Pearson correlation coefficient is applied. This method assesses the linear correlation between morphometric indicators and key hydrological outputs such as peak discharge and time of concentration. The analysis helps identify the most influential parameters and reveals other significant associations, enabling the classification of morphometric factors according to their impact on hydrological behavior.

The Pearson correlation coefficient (r), a unitless measure, quantifies the strength and direction of the linear relationship between two variables and can be calculated using the standard formula described by Lee Rodgers J, et al. [60].

$$r = \frac{\sum(X_i - \bar{X})(Y_i - \bar{Y})}{\sqrt{[\sum(X_i - \bar{X})^2 * \sum(Y_i - \bar{Y})^2]}} \quad (1)$$

where

- Xi represents the individual values of the morphometric parameters used to evaluate flood hazard potential across the basins.
- Yi denotes the corresponding hydrological parameter values, such as peak flow or time of concentration.
- $\bar{X}$ is the mean of the morphometric parameters.
- $\bar{Y}$ is the mean of the hydrological parameters.

The Pearson correlation coefficient (r), which ranges from -1 to 1, quantifies the strength and direction of the linear relationship between two variables. A value of r = 1 signifies a perfect positive correlation, while r = -1 indicates a perfect negative correlation, and r = 0 denotes no linear relationship. This statistical metric is essential for determining which morphometric parameters exert the most

influence on hydrological responses, particularly in the context of flash flood susceptibility. In this study, Pearson correlation analysis was applied to morphometric data from the Northwest Coast of Egypt to classify parameters based on their relationship with flood hazard indicators, as summarized in Table 8. The results indicate that the degree of correlation between morphometric attributes and stormflow generation is influenced by regional geomorphological characteristics. Several parameters, such as basin area (Ab), perimeter (P), main flow direction (MFD), number of streams (Nu), basin texture (T), and circularity ratio (C), demonstrate strong positive correlations with hydrological response, with coefficients exceeding 0.9. In contrast, certain variables exhibit strong negative correlations, such as shape, (MFS), and (MSS). Overall, 28 of the 44 assessed morphometric parameters significantly affect flash flood hazard levels, highlighting their importance in flood risk assessment and basin management.

Table 9. Pearson correlation results on the Northwest Coastof Egypt.

Hydrological Parameters	$\mathbf{A_b}$	BS	AOFD	$\mathbf{L_b}$	P	SHAPE	SIN	AVEL	MFD	MFS	MSL	MSS	CORSTR	CSD	CSS	$\boldsymbol{N_u}$
Peak (m^3/sec)	0.981	0.312	0.202	0.678	0.903	-0.316	0.510	0.334	0.838	-0.748	0.404	-0.748	0.054	0.642	-0.658	0.978
Runoff Volume (m^3)	1.000	0.179	0.179	0.746	0.969	-0.201	0.547	0.486	0.915	-0.815	0.540	-0.815	0.170	0.752	-0.662	0.999
Time of Concentration (hr.)	0.941	0.076	0.248	0.906	0.979	0.134	0.379	0.729	0.993	-0.941	0.613	-0.941	0.177	0.906	-0.757	0.944
Mean	0.974	0.189	0.209	0.777	0.950	-0.128	0.478	0.517	0.916	-0.834	0.519	-0.834	0.134	0.767	-0.692	0.974
Hydrological Parameters	L_u	L_{ur}	R_b	ρ	P_r	W_b	L_{ar}	K	F_f	SH	I_{sh}	R_e	R_c	R_{cn}	T	C_c
Peak (m^3/sec)	0.436	-0.660	-0.556	-0.579	0.958	0.957	0.972	-0.313	0.220	-0.302	0.220	0.248	-0.302	-0.302	0.940	0.304
Runoff Volume (m^3)	0.522	-0.649	-0.528	-0.599	0.917	0.944	0.994	-0.199	0.120	-0.474	0.120	0.145	-0.473	-0.473	0.911	0.477
Time of Concentration (hr.)	0.731	-0.508	-0.405	-0.483	0.841	0.784	0.964	0.137	-0.204	-0.672	-0.204	-0.183	-0.677	-0.677	0.861	0.662
Mean	0.563	-0.606	-0.496	-0.553	0.905	0.895	0.977	-0.125	0.045	-0.483	0.045	0.070	-0.484	-0.484	0.904	0.481
Hydrological Parameters	D_d	F_s	C	D_i	I_f	H	R_{hl}	R_n	R_a	R_{hp}	D_{is}	MR_n				
Peak (m^3/sec)	-0.942	0.156	0.974	0.979	-0.894	0.269	-0.572	-0.819	0.628	-0.779	-0.510	-0.806				
Runoff Volume (m^3)	-0.913	0.237	0.968	0.979	-0.853	0.315	-0.647	-0.770	0.710	-0.854	-0.600	-0.811				
Time of Concentration (hr.)	-0.812	0.422	0.840	0.862	-0.724	0.392	-0.835	-0.634	0.888	-0.943	-0.811	-0.805				
Mean	-0.889	0.272	0.927	0.940	-0.823	0.325	-0.685	-0.741	0.742	-0.859	-0.640	-0.807				

To determine the hazard degree of each basin, the following steps should be followed [55]:

1- Calculate the weight of morphometric parameters of each basin using the Davis equation, then multiply it by the Pearson correlation coefficient to determine the real effect of the hydrological parameters [61]. The Davis equation is as follows:

$$Weight\ of\ Parameter = \left(\frac{4(X_i - X_{min})}{(X_{max} - X_{min})} + 1\right) * \quad (2)$$

2- Sum the weight of all the morphological parameters of each basin separately.

3- The basins must be divided into 5 intervals starting from 1 (lowest hazard) to 5 (highest hazard) and assigned to all parameters. The hazard scale is shown in table 9.

Table 10. Hazard scale number [56].

Total SRF	Class of the Hazard degree	Symbol of class
R1	Low	L
R2	Moderately Low	ML
R3	Moderate	M
R4	Moderately High	MH
R5	High	H

4- Calculate the range and end of each interval using the following equations:

$$Range = (R_5 - R_1)/n \quad (3)$$

$$R_n = R_{n-1} + Range \quad (4)$$

where

$R_1 = \min \text{total weight}$

$R_5 = \max total\ weight$

$n = \text{no. of classes}$

5- Specify the Hazard degree by determining in what interval each basin is located.

Table 10 presents the results of the flood hazard degree analysis, summarizing the ranking scores assigned to morphometric parameters across the seven basins based on their statistical relationship, either direct or inverse, with flood hazard potential. Two assessment methods are employed: The first considers all morphometric parameters (Table 10-a), while the second focuses only on those with a significant correlation (absolute Pearson correlation coefficient |r| > 0.5) with hydrological response indicators (Table 10-b). The computed hazard scores integrate the standardized weights of each parameter and the direction and magnitude of their correlation with flood-prone behavior, offering a comprehensive measure of each basin's susceptibility. The analysis highlights Wadi Khreisa (Basin 5) as the most flood-prone basin in the study area, consistently ranking highest in both evaluation methods.

Table 11. Value of Hazard degree for all basins on the Northwest Coastof Egypt.

(a) For all parameters			(b) For parameters with effect >= |0.5|		
Ba	Total Weight	Degree	Ba	Total weight for risk >= |0.5|	Degree
1	17.62249	M	1	19.19753	M
2	3.51885	ML	2	4.36127	ML
3	11.07767	M	3	8.97675	M
4	28.89184	MH	4	28.57454	MH
5	62.43711	H	5	55.65536	H
6	-9.58758	ML	6	-13.20902	L
7	-28.10165	L	7	-23.41817	L
Min	-28.10165		Min	-23.41817	
Max	62.43711		Max	55.65536	
Range	18.10775153		Range	15.8147062	

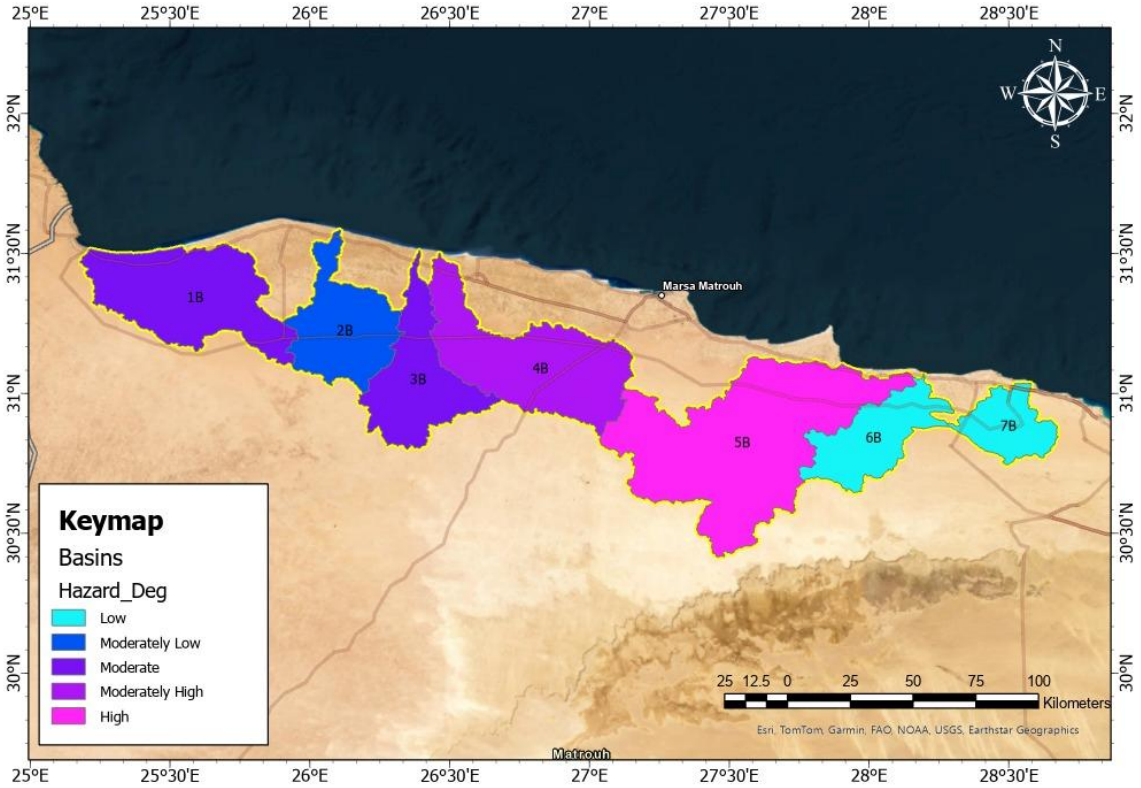

Figure 20. Flood hazard and physical susceptibility levels for the selected subbasins using all parameters.

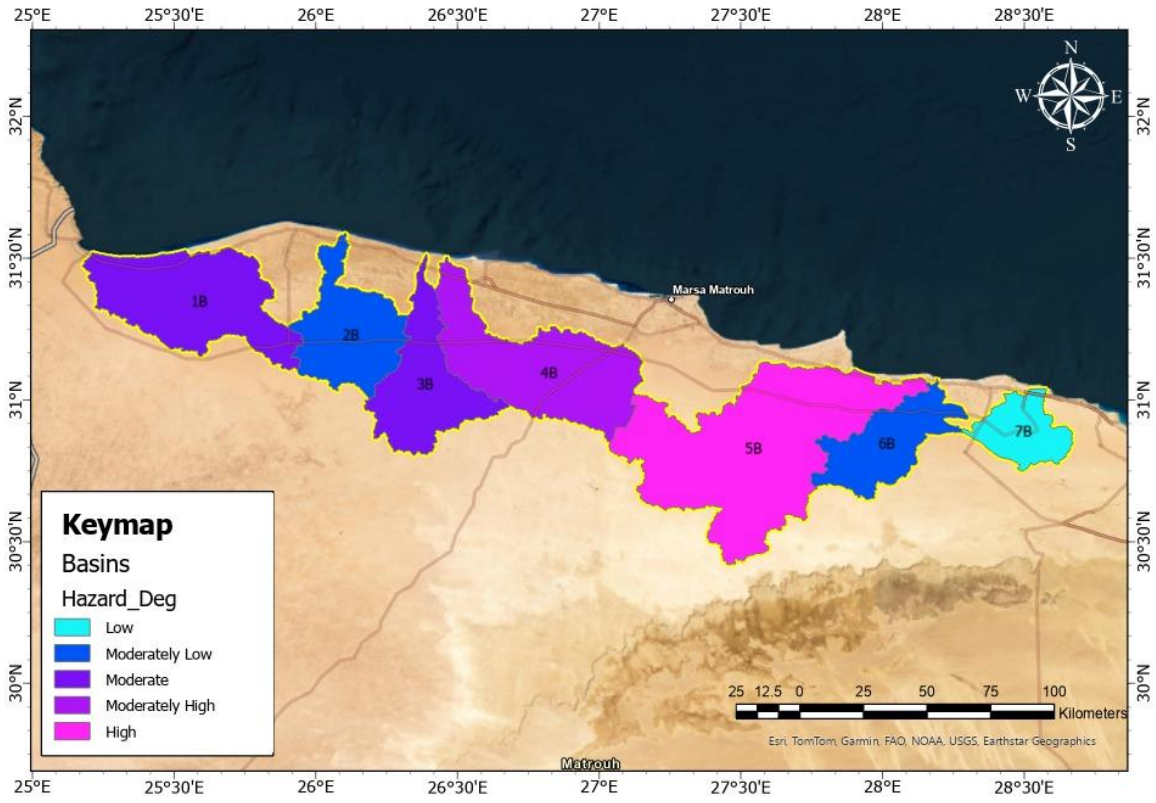

Figure 21. Flood hazard and physical susceptibility levels for the selected subbasins using parameter's weight >|0.5|.

This result is corroborated by the spatial visualization in Figures 21 and 22, which demonstrate the varying flood hazard and physical susceptibility levels across the seven delineated basins along Egypt's Northwest Coast. Basin 5 (Wadi Khreisa), highlighted in red, stands out as the most hazardous zone, exhibiting high flood susceptibility compared to the surrounding basins. This spatial pattern aligns with the basin's geomorphological attributes, including high stream frequency, dense drainage networks, moderate basin compactness, and substantial relief, which collectively enhance runoff concentration and peak discharge potential. In contrast, Basins 1B and 7B, which occupy the western and eastern portions of the study area, display lower hazard degrees due to gentler slopes, larger basin areas, and higher infiltration potential. The gradient of hazard from west to east reflects the combined influence of topography, morphometric configuration, and rainfall variability, reinforcing the integrated role of geomorphology in shaping basin hazard to flash floods.

4.2. Hazard and susceptibility assessment analysis

The hazard and susceptibility of the Northwest coast basins is evaluated by integrating hydrological, hydraulic, and morphological perspectives. While the hydrological analysis identifies Basin 2 (Wadi El-Harika) as generating the highest runoff peaks, more than 180 m^3/s in 2009–2020 and more than 800 m^3/s under the 100-year return period, the hydraulic modeling highlights Basin 5 (Wadi Khreisa) as the most hazardous, with maximum flood depths reaching 6 m and 30 m for the respective periods.

Table 12 represents a comparative morphometric parameter of Basin 2 (Wadi El-Harika) and

Basin 5 (Wadi Khreisa), highlighting the role of drainage geometry, relief, and texture in shaping basin hazard. Despite Basin 2's higher runoff volumes, Basin 5 exhibits greater susceptibility due to its higher drainage density, stream frequency, and basin texture, which promote rapid flow concentration and localized inundation. In arid coastal settings, sparse vegetation and low soil infiltration amplify runoff generation, while low-gradient downstream plains and proximity to the coast restrict flow evacuation, extending flood duration. These physical controls explain why Basin 5 experiences greater flood depths and spatial extent despite moderate runoff peaks. These discrepancies demonstrate that high runoff volumes do not necessarily translate into greater flood severity, as topographic and morphological controls strongly influence inundation depth and spatial extent. Consequently, Basin 5 emerges as the most vulnerable basin despite its moderate runoff peaks.

This multidimensional assessment underscores the importance of coupling hydrological and hydraulic outputs with geomorphological parameters to capture basin-specific flood hazard. The results provide a more robust basis for targeted flood mitigation, land-use planning, and water resource management on Egypt's Northwest Coast.

Table 12. Comparative morphological parameters for Basins 2 and 5.

Parameters		Basin 2 (Wadi El-Harika)	Basin 5 (Wadi Khreisa)
Main Basin Parameter	(A_b)	1295.64	3831.53
	(L_b)	65349.98	88294.08
	(P)	307467.33	602894
Geometric Parameters	Pr	4213.9	6355.2
	Wb	19826.2	43395.1
	Lar	410788.9	787320.2
	Kf	0.30338	0.49148
	T	0.02349	0.03355
	Cc	2.42677	2.76711
Drainage parameters	Nu	7223	20226
	Lu	3328539	3048142
Relief Parameters	Z	219.5	263.8
	z	0.5	4.3
	H	219	259.5
	Ra	219.5	263.8
Drainage Texture	Fs	5.26E-06	5.28E-06
	C	472.807	1257.005
	Di	0.00248	0.00663

Based on these results, flood hazard and physical susceptibility assessment provide critical guidance for water resource planning and sustainable development across the Northwest Coast. Basin 2 (Wadi El-Harika), with its high runoff potential, requires careful management at outlet zones, while its upstream regions are more suitable for rain-fed agriculture. Basins 5 and 6, characterized by moderate runoff, also present opportunities for agricultural use but necessitate monitoring of localized flood risks. In contrast, the coastal corridor between Fuka and Sidi Barrani is identified as a low-hazard and susceptibility zone, making it more suitable for investment and tourism, given the limited flood hazards associated with smaller basins. For Basin 5, targeted mitigation measures, such as upstream

afforestation, soil conservation, and the installation of culverts to protect infrastructure, are essential to reduce flood impacts and enhance resilience. Collectively, these findings emphasize the importance of basin-specific management strategies and highlight the need for adaptive flood governance frameworks to safeguard coastal infrastructure, ecosystems, and socio-economic development.

Although instrumental flood records are limited for the Northwest Coast, observations and remote sensing provide evidence of significant flooding in the region. For instance, an unexpected flood event in Mersa Matruh in October 2023 caused notable inundation despite rainfall that did not exceed typical design return periods, highlighting the influence of local topography and drainage characteristics on flood generation in arid coastal basins [62]. These observations are consistent with our findings for Basin 5, where insufficient drainage infrastructure, malfunctioning flood protection measures, and basin morphology likely amplify flooding. This underscores the critical importance of prioritizing very high- and high-risk zones. In these areas, effective flood mitigation strategies may include enhancing drainage networks, constructing flood barriers (e.g., dikes or small dams), and implementing early warning systems.

5. Conclusions

In this study, we present a flood hazard and susceptibility assessment of flash floods across Egypt's Northwest Coast by combining geomorphological, hydrological, and hydraulic analyses using advanced tools such as GIS, Remote Sensing, WMS, HEC-HMS, and HEC-RAS. The analysis of seven major basins revealed substantial variability in vulnerability, driven not only by runoff volumes but also by basin morphology and floodplain characteristics. While Basin 2 (Wadi El-Harika) generated the highest runoff, Basin 5 (Wadi Khreisa) was identified as the most susceptible, exhibiting extreme flood depths due to unfavorable morphometric parameters, limited drainage capacity, and topographic flattening. Morphometric and hydrological evaluations highlighted 28 key parameters influencing flood risk, while rainfall trend analysis confirmed an intensification of precipitation over recent decades, reflecting climate change impacts. Hydraulic modeling further showed that some basins with moderate runoff are prone to considerable flood depths, emphasizing the complex interaction between topography, drainage networks, and runoff behavior. These findings demonstrate that vulnerability is a multidimensional outcome shaped by the interaction of hazard intensity, basin susceptibility, and local adaptive capacity.

In light of these findings, Basin 2 (Wadi El-Harika) requires careful outlet management due to its high runoff, while upstream areas and Basins 5 and 6 are more suitable for rain-fed agriculture. The coastal stretch between Fuka and Sidi Barrani appears safe for tourism and investment, given the minimal flood threats from small basins. For high-risk basins, particularly Basin 5, targeted interventions such as upstream afforestation, culvert construction, and improved drainage infrastructure are recommended to protect infrastructure and enhance resilience.

Future climate change, particularly increasing extreme rainfall intensity and variability, may modify flood susceptibility patterns in the Northwest coast basins, emphasizing the need for dynamic map updates and adaptive flood risk management strategies. In addition, researchers should extend this framework by integrating coastal inundation drivers, such as storm surge and sea-level rise, with fluvial flood susceptibility to assess compound flooding along Egypt's Northwest Coast.

Overall, the study underscores the importance of basin-specific and climate-resilient flood management strategies that integrate structural and non-structural measures, land-use planning, and

early warning systems. By providing a scalable framework for adaptive flood risk management, these results contribute to sustainable water resource planning, resilient urban development, and informed policymaking to address the growing challenges of climate-induced hydrological extremes along Egypt's Northwest Coast.

Use of AI tools declaration

The authors declare they have not used Artificial Intelligence (AI) tools in the creation of this article.

Conflict of interest

The authors declare that there is no conflict of interest.

References

1. WMO, 2019. Flash Flood Guidance System (FFGS) World Meteorological Organization (WMO). https://community.wmo.int/en/hydrology-and-water-resources/flash-flood-guidance-system-ffgs-global-coverage
2. UNDRR (*2025*) United Nation Office for Disaster Risk Reduction. Retrieved from: https://www.undrr.org/quick/78571
3. *IPCC, 2023: Climate Change 2023: Synthesis Report. Contribution of Working Groups I, II and III to the Sixth Assessment Report of the Intergovernmental Panel on Climate Change [Core Writing Team, H. Lee and J. Romero (eds.)]. IPCC, Geneva, Switzerland.* (P. Arias, M.Bustamante, I. Elgizouli, G. Flato, M. Howden, C. Méndez-Vallejo, J. J. Pereira, R. Pichs-Madruga, S. K. Rose, Y. Saheb, R. Sánchez Rodríguez, D. Ürge-Vorsatz, C. Xiao, N. Yassaa, J. Romero, J. Kim, E. F. Haites, Y. Jung, R. Stavins, … C. Péan, Eds.) https://doi.org/10.59327/IPCC/AR6-9789291691647
4. Al Azzam, N., & Al Kuisi, M. (2021) Determination of Flash Floods Hazards and Risks for Irbid Governorates Using Hydrological and Hydraulic Modelling. *Jordan J Earth Environ Sci*
5. Negm AM (2020) *Flash Floods in Egypt*. Springer International Publishing. https://doi.org/10.1007/978-3-030-29635-3
6. Arnous M O, El-Rayes A E, El-Nady H, et al. (2022) Flash flooding hazard assessment, modeling, and management in the coastal zone of Ras Ghareb City, Gulf of Suez, Egypt. *J Coast Conserv* 26: 77. https://doi.org/10.1007/s11852-022-00916-w
7. Creutin J D, Borga M (2003) Radar hydrology modifies the monitoring of flash-flood hazard. *Hydrol Process* 17: 1453–1456. https://doi.org/10.1002/hyp.5122
8. Kundzewicz ZW, Jania JA (2007) *GEOGRAPHIA POLONICA EXTREME METEOROLOGICAL AND HYDROLOGICAL EVENTS IN POLAND EDITORS* 80. www.arspolona.com.pl
9. Mazzorana B, Hübl J, Fuchs S (2009) Natural Hazards and Earth System Sciences Improving risk assessment by defining consistent and reliable system scenarios. *Hazards Earth Syst Sci* 9: 145–159. www.nat-hazards-earth-syst-sci.net/9/145/2009/

10. Khan M Y A, ElKashouty M, Subyani A M, et al. (2022) Flash Flood Assessment and Management for Sustainable Development Using Geospatial Technology and WMS Models in Abha City, Aseer Region, Saudi Arabia. *Sustainability* 14: 10430. https://doi.org/10.3390/su141610430
11. Mahmood S, Rahman A (2019) Flash flood susceptibility modeling using geo-morphometric and hydrological approaches in Panjkora Basin, Eastern Hindu Kush, Pakistan. *Environ Earth Sci* 78: 43. https://doi.org/10.1007/s12665-018-8041-y
12. Mahmood S, Rani R (2018) Extent of 2014 Flood Damages in Chenab Basin Upper Indus Plain. *Nat Hazards Risk Assess Vulnerability Reduct* 2018: 75. https://doi.org/10.5772/intechopen.79687
13. Hashmi H N, Siddiqui Q T M, Ghumman A R, et al. (2012) A critical analysis of 2010 floods in Pakistan. *Afr J Agric Res* 7: 1054–1067. https://doi.org/10.5897/ajarx11.036
14. Santangelo N, Santo A, Di Crescenzo G, et al. (2011) Flood susceptibility assessment in a highly urbanized alluvial fan: The case study of Sala Consilina (southern Italy). *Nat Hazards Earth Syst Sci* 11: 2765–2780. https://doi.org/10.5194/nhess-11-2765-2011
15. Horton RE (1945) Erosional development of streams and their drainage basins; hydrophysical approach to quantitative morphology. *Bull Geol Soc Am 56*: 275–370.
16. Strahler A N (1964) Quantitative geomorphology of drainage basins and channel networks. *Handbook of Appl Hydrol* 1964.
17. Strahler A N (1957) Quantitative analysis of basin geomorphology. *Trans Am Geophys Union* 38: 913–920.
18. Sadek M, Li X, Mostafa E, et al. (2020) Low-Cost Solutions for Assessment of Flash Flood Impacts Using Sentinel-1/2 Data Fusion and Hydrologic/Hydraulic Modeling: Wadi El-Natrun Region, Egypt. *Adv Civil Eng* 2020: 1039309. https://doi.org/10.1155/2020/1039309
19. El Osta M M, El Sabri M S, Masoud M H (2016) Estimation of flash flood using surface water model and GIS technique in Wadi El Azariq, East Sinai, Egypt. *Nat Hazards Earth Syst Sci Discuss* 2016: 1–51. https://doi.org/10.5194/nhess-2016-311
20. Shuka K A M, Wang K, Abubakar G A, et al. (2024) Impact of Structural and Non-Structural Measures on the Risk of Flash Floods in Arid and Semi-Arid Regions: A Case Study of the Gash River, Kassala, Eastern Sudan. *Sustainability 16*: 1752. https://doi.org/10.3390/su16051752
21. Abdel-Fattah M, Saber M, Kantoush S A, et al. (2017) A hydrological and geomorphometric approach to understanding the generation of wadi flash floods. *Water* 9: 553. https://doi.org/10.3390/w9070553
22. Abdelgawad A G, Helal E, Sobeih M F, et al. (2024) Flood hazard mapping using a GIS-based morphometric analysis approach in arid regions, a case study in the Red Sea Region, Egypt. *Appl Water Sci* 14: 81. https://doi.org/10.1007/s13201-024-02130-5
23. Ahmed A, Hewa G, Alrajhi A (2021) Flood susceptibility mapping using a geomorphometric approach in South Australian basins. *Nat Hazards* 106: 629–653. https://doi.org/10.1007/s11069-020-04481-z
24. Alqahtani F, Qaddah A A (2019) GIS digital mapping of flood hazard in Jeddah–Makkah region from morphometric analysis. *Arab J Geosci* 12: 199. https://doi.org/10.1007/s12517-019-4338-8
25. Bhat M S, Alam A, Ahmad S, et al. (2019) Flood hazard assessment of upper Jhelum basin using morphometric parameters. *Environ Earth Sci* 78: 54. https://doi.org/10.1007/s12665-019-8046-1

26. Gabriel A T, Yusuf M B, Bwadi B E, et al. (2020) Morphometric Analysis and Flash Floods Assessment of River Taraba Basin in Taraba State, Nigeria. *Eur Sci J* 16: 158–175. https://doi.org/10.19044/esj.2020.v16n20p158
27. Hagos Y G, Andualem T G, Yibeltal M, et al. (2022) Flood hazard assessment and mapping using GIS integrated with multi-criteria decision analysis in upper Awash River basin, Ethiopia. *Appl Water Sci* 12: 148. https://doi.org/10.1007/s13201-022-01674-8
28. Adnan M S G, Dewan A, Zannat K E, et al. (2019) The use of basin geomorphic data in flash flood susceptibility zoning: a case study of the Karnaphuli and Sangu river basins of Bangladesh. *Nat Hazards* 99: 425–448. https://doi.org/10.1007/s11069-019-03749-3
29. Sarkar D, Mondal P (2020) Flood vulnerability mapping using frequency ratio (FR) model: a case study on Kulik river basin, Indo-Bangladesh Barind region. *Appl Water Sci* 10: 17. https://doi.org/10.1007/s13201-019-1102-x
30. Hamedo N, Mohamed Aly M, Khaled Mostafa M, et al. (2021) Flash Flood Management in Arid Region: A Case Study Urban Bani Wasil Village, Sohag Governorate. *Eng Res J* 169: 130–146.
31. Diwate P, Lavhale P, Pande C B, et al. (2025) Evaluating flood dynamics and effects in Nagpur city using remote sensing and Shannon's entropy analysis. *Sci Rep 15*: 4900. https://doi.org/10.1038/s41598-025-86801-6
32. Khan M Y A, ElKashouty M, Subyani A M, et al. (2022) Flash Flood Assessment and Management for Sustainable Development Using Geospatial Technology and WMS Models in Abha City, Aseer Region, Saudi Arabia. *Sustainability* 14: 10430. https://doi.org/10.3390/su141610430
33. Dong Z, Liu H, Hu H, et al. (2022) Future projection of seasonal drought characteristics using CMIP6 in the Lancang-Mekong River Basin. *J Hydrol 610*: 127815. https://doi.org/10.1016/j.jhydrol.2022.127815
34. Harris I, Osborn T J, Jones P, et al. (2020) Version 4 of the CRU TS monthly high-resolution gridded multivariate climate dataset. *Sci Data* 7: 109. https://doi.org/10.1038/s41597-020-0453-3
35. Mashaly J, Ghoneim E (2018) Flash flood hazard using optical, radar, and stereo-pair derived DEM: Eastern desert, Egypt. *Remote Sens* 10: 1204. https://doi.org/10.3390/rs10081204
36. Abd-Elhamid H F, Fathy I, Zeleňáková M (2018) Flood prediction and mitigation in coastal tourism areas, a case study: Hurghada, Egypt. *Nat Hazards* 93: 559–576. https://doi.org/10.1007/s11069-018-3316-x
37. Fathy I, Zeleňáková M, Abd-Elhamid H F (2020) Highways protection from flood hazards, a case study: New Tama road, KSA. *Nat Hazards* 103: 479–496. https://doi.org/10.1007/s11069-020-03996-9
38. Fathy I, Adel H, Ramadan E M, et al. (2025) Management Of Soil Erosion and Sediment Yield In Semi-Arid Regions, A Case Study Of Wadi Sudr Basin, South Sinai, Egypt. *Carpath J Earth Environ Sci* 20: 307–322. https://doi.org/10.26471/cjees/2025/020/335
39. Fathy I, Ahmed A, Abd‐Elhamid H F (2021) Integrated management of surface water and groundwater to mitigate flood risks and water scarcity in arid and semi-arid regions. *J Flood Risk Manag* 14: e12720. https://doi.org/10.1111/jfr3.12720
40. GIOVANNI-NASA (2025) https://giovanni.gsfc.nasa.gov/giovanni/

41. *Global Weather Data for SWAT*. The National Centers for Environmental Prediction. Retrieved June 12, 2020, from https://globalweather.tamu.edu/
42. National Oceanic and Atmospheric Administration. (2023, April 14) JetStream Max: Addition Köppen-Geiger Climate Subdivisions. https://www.noaa.gov/jetstream/global/climate-zones/jetstream-max-addition-k-ppen-geiger-climate-subdivisions
43. Esri (2020) *A new land cover map of the world*. Esri 2020 Land Cover Downloader. Retrieved June 27, 2021, from https://livingatlas.arcgis.com/landcover/_
44. FAO (2017) *Digital Soil Map of the World*. Food and Agriculture Organization of the United Nations. Retrieved 2020 from http://www.fao.org/soils-portal /
45. FAO (2021) *AQUASTAT Climate Information Tool (2009–2020)*. Food and Agriculture Organization of the United Nations. Retrieved from http://www.fao.org/aquastat/
46. CGIAR-CSI (2020) *SRTM data*. CGIAR Consortium for Spatial Information. Retrieved November 18, 2020, from https://srtm.csi.cgiar.org/srtmdata/
47. Horton R E (1932) Erosional development of streams and their drainage basins; hydrophysical approach to quantitative morphology. *Bulletin of the Geological Society of America* 63: 275–370.
48. Schumm S A (1956) Evolution of drainage systems and slopes in badlands at Perth Amboy, New Jersey. *Bulletin of the Geological Society of America* 67: 597–646.
49. Hack J T (1957) Studies of longitudinal stream profiles in Virginia and Maryland. US Government Printing Office, 1957.
50. Chorley R J (1957) A new standard for estimating drainage basin shape. *Amer Jour Sci* 255: 138–141.
51. Strahler A N (1964) Quantitative geomorphology of drainage basin and channel networks. Handbook of applied hydrology, 1964.
52. Dinagara Pandi P, Thena T, Nirmal B, et al. (2017) Morphometric analyses of Neyyar River Basin, southern Kerala, India. *Geology Ecol Landsc* 1: 249–256.
53. SMITH K G (1950) STANDARDS FOR GRADING TEXTURE OF EROSIONAL TOPOGRAPHY. *Amer J Sci*
54. Gupta B (1995) *Runoff. In: Engineering Hydrology.*
55. Strahler A N (1952) Hypsometric (Area-Altitude) Analysis Of Erosional Topography. America: Bulletin Of The Geological Society Of America. *Geol Soc Am Bull* 63: 1117–1142.
56. Melton M A (1957) An analysis of the relations among elements of climate, surface properties, and geomorphology. New York: Department of Geology,Columbia University.
57. Pareta K, Pareta U (2011) Quantitative morphometric analysis of a watershed of Yamuna basin, India using ASTER (DEM) data and GIS. *International journal of Geomatics and Geosciences* 2: 248–269.
58. Wilford D J, Sakals M E, Innes J L, et al. (2004) *Recognition of debris flow, debris flood and flood hazard through basin morphometrics.* Springer-Verlag.
59. Faniran A (1962) *The Index of Drainage Intensity - A Provisional New Drainage Factor.* Australia: *Aust J Sci*
60. Lee Rodgers J, Nicewander W A. (1988) Thirteen ways to look at the correlation coefficient. *The American Statistician* 42: 59–66. https://doi.org/10.1080/00031305.1988.10475524
61. Davis J C, Sampson R J (1975) Statistics *and data analysis in geology*. New York: John Wiley & Sons, The University of Kansas.

62. Ezz Hesham (2025) UNEXPECTED FLOODING IN MERSA MATRUH, EGYPT INVESTIGATING CAUSES, HYDROLOGICAL ANALYSIS, AND FLOOD RISK ASSESSMENT. 61: 371–399.

AIMS Press